



RESEARCH ARTICLE

10.1029/2022JD038328

Key Points:

- First combined observations of optical activity, cloud microphysics and lightning related to blue corona discharges in a tropical cyclone
- The source depth of the blue corona discharges inside the cloud estimated from optical and radio observations agree well
- Blue corona discharges are related to a strong updraft, high-density large ice particles and an increase in the total lightning rate

Supporting Information:

Supporting Information may be found in the online version of this article.

Correspondence to:









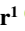




D. Li,
dongshuai@space.dtu.dk

Citation:

Li, D., Neubert, T., Husbjerg, L. S., Zhu, Y., Chanrion, O., Lapiere, J., et al. (2023). Observation of blue corona discharges and cloud microphysics in the top of thunderstorm cells in cyclone Fani. *Journal of Geophysical Research: Atmospheres*, 128, e2022JD038328. <https://doi.org/10.1029/2022JD038328>

Received 8 DEC 2022
Accepted 18 OCT 2023

Observation of Blue Corona Discharges and Cloud Microphysics in the Top of Thunderstorm Cells in Cyclone Fani

Dongshuai Li¹ , Torsten Neubert¹ , Lasse Skaaning Husbjerg¹ , Yanan Zhu² , Olivier Chanrion¹ , Jeff Lapiere² , Alejandro Luque³ , Christoph Köhn¹ , Matthias Heumesser¹ , Krystallia Dimitriadou^{1,4} , Martin Stendel⁵ , Eigil Kaas^{5,6} , Emilie Petrea Petajamaa Wiinberg Olesen¹, Feifan Liu⁷, Nikolai Østgaard⁸ , and Víctor Reglero⁹

¹National Space Institute, Technical University of Denmark (DTU Space), Kongens Lyngby, Denmark, ²Earth Networks, Germantown, MD, USA, ³Instituto de Astrofísica de Andalucía (IAA), CSIC, Granada, Spain, ⁴DTU Wind and Energy Systems, Roskilde, Denmark, ⁵Danish Meteorological Institute, Copenhagen, Denmark, ⁶Niels Bohr Institute, University of Copenhagen, Copenhagen, Denmark, ⁷CAS Key Laboratory of Geospace Environment, University of Science and Technology of China, Hefei, China, ⁸Department of Physics and Technology, Birkeland Centre for Space Science, University of Bergen, Bergen, Norway, ⁹Image Processing Laboratory, University of Valencia, Valencia, Spain

Abstract Blue corona discharges are often observed at the top of thunderclouds. They are bursts of streamers, but the cloud conditions that enable them are not well known. Here we present observations by the Atmosphere-Space Interactions Monitor (ASIM) of 92 discharges during its ~ 1 min pass over tropical cyclone Fani in the Bay of Bengal from 20:10:55 to 20:12:05 UTC on 30 April 2019. The discharges were observed in convective cells forming in the rainbands of the cyclone where Convective Available Potential Energy reached $\sim 6,000$ J kg⁻¹. The Cloud-Aerosol Lidar and Infrared Pathfinder Satellite Observation satellite passed over one of the cells ~ 12 min after ASIM from 20:23:58 to 20:24:14 UTC. It measured the cloud microphysics related to the discharges and indicated they occurred in a convection region with the cloud top overshooting for over 20 min. The updraft lifted ice particles to lower stratospheric altitudes and formed the gullwing-shaped cirrus. The discharges are found at an average altitude of ~ 16 km where the cloud environment contained $\sim 2 \times 10^7$ m⁻³ ice particles with ~ 50 μ m radius, resulting in a photon mean free path of ~ 3 m. Around 20% of the blue corona discharges coincide with Narrow Bipolar Events identified from the Earth Networks Total Lightning Network. Our observations suggest that the overshooting cloud top formed by deep convection and a surge in lightning activity facilitated conditions for the blue corona discharges. This work provides the first-ever estimate of important microphysical parameters related to blue corona discharges based on data measurements, establishing a reference for future empirical and theoretical studies.

Plain Language Summary Blue corona discharges are bursts of streamer discharges often observed at the top of thunderclouds, but the conditions in the clouds that generate them are not well understood. In this study, we discuss observations of blue corona discharges in convective cells detected by the Atmosphere-Space Interactions Monitor on the International Space Station as it passed over cyclone Fani in the Bay of Bengal. For the first time, we have observations of the cloud particle characteristics at the cloud tops taken shortly afterward by the Cloud-Aerosol Lidar and Infrared Pathfinder Satellite Observation satellite, which are related to the blue corona discharges. The observations indicate that the blue corona discharges may be Narrow Bipolar Events associated with strong convection in cloud cells reaching into the stratosphere. The cloud microphysical parameters related to blue corona discharges are important for future empirical studies and for theoretical models and simulations.

1. Introduction

The bright luminous channel of lightning is a highly ionized plasma with high electrical conductivity. The plasma channel of lightning leaders is so hot that molecular oxygen dissociates into atomic oxygen, often detected at the atomic O I line in 777.4 nm (Blakeslee et al., 2020; Christian et al., 1989; Goodman et al., 2013; Grandell et al., 2010; Yang et al., 2017). Streamers are low-density, cold plasma filaments that emerge from propagating ionization fronts (da Silva & Sao Sabbas, 2013; Ebert & Sentman, 2008; Luque & Ebert, 2009; Nijdam

© 2023. The Authors.

This is an open access article under the terms of the [Creative Commons Attribution License](https://creativecommons.org/licenses/by/4.0/), which permits use, distribution and reproduction in any medium, provided the original work is properly cited.

et al., 2020). Bursts of streamers may be generated without a leader, or may be formed in the high electric field region that precedes the leader formation (da Silva & Pasko, 2013; Raizer & Allen, 1991). In the atmosphere, at altitudes up to about 50 km, they appear blue with strong emissions at 337 nm from the second positive system of N_2 (N_2^2P) in the near-ultraviolet band (Chanrion et al., 2019; Gordillo-Vázquez & Pérez-Invernón, 2021; Montanyà et al., 2021; Raizer & Allen, 1991; Walker & Christian, 2019) with weak or no emissions in the atomic oxygen band of lightning leaders at 777.4 nm.

Observing blue corona discharges, especially those occurring inside or near the top layer of clouds, is challenging when attempted from the ground due to scattering and absorption in the cloud. As a result, they are best observed from space. The Imager of Sprites and Upper Atmospheric Lightning on FormoSat-2 (Chou et al., 2018; F. Liu et al., 2018) reported blue luminous events that radiated unambiguous middle ultraviolet (UV) to blue emissions (230–450 nm) and also contained dim red emissions (623–754 nm). In 2015, an astronaut onboard the International Space Station (ISS) also made observations of blue corona discharges with rates of around 120 per min observed in a single storm (Chanrion et al., 2017). The Atmosphere-Space Interactions Monitor (ASIM) more recently installed on the ISS (Neubert et al., 2019) provides a unique opportunity for systematic monitoring of these phenomena on a global scale.

We refer to the discharges with dominant 337 nm emission, as observed by ASIM, as blue corona discharges. We include other similar phenomena reported in the literature into the category, such as *small blue surface discharges* (also called *blue glimpses*), *pixies* and *gnomes* which occur in-cloud or close to the cloud-top layer within a few kilometers (Chanrion et al., 2017; Gordillo-Vázquez & Pérez-Invernón, 2021; Lyons et al., 2003; Neubert et al., 2021; Pasko, 2008; Wescott et al., 1996, 2001), or *blue starters* and *blue jets* that emerge from the cloud tops reaching altitudes of up to tens of kilometers (Wescott et al., 1996, 2001). However, the detailed mechanisms underlying these different types of blue luminous discharges remain to be fully understood.

Recent studies have linked blue corona discharges to short-duration (10–20 μ s) bipolar pulses with strong Very High Frequency radiation, called Narrow Bipolar Events (NBEs) (Chou et al., 2018; Li et al., 2021, 2022b; F. Liu et al., 2018, 2021a, 2021b; Smith et al., 1999, 2004; Soler et al., 2020; Wu et al., 2012). NBEs are thought to be produced by localized and fast propagating streamers, known as fast breakdown (Li et al., 2022a; N. Liu et al., 2019; Rison et al., 2016; Tilles et al., 2019). They are likely to occur independently from other lightning discharges within tens of milliseconds or at the onset of lightning leader formation (Kostinskiy et al., 2020; López et al., 2022; Lyu et al., 2019; Marshall et al., 2019; Rison et al., 2016). The relationship between blue corona discharges and NBEs is still under investigation (Li et al., 2022b, 2023).

There is a growing number of studies of blue corona discharges based on ASIM measurements (Bai et al., 2023; Dimitriadou et al., 2022; Husbjerg et al., 2022; Li et al., 2021, 2022b; F. Liu et al., 2021a; Soler et al., 2020, 2021). On a global scale, they are estimated to occur at a rate of about 11 s^{-1} at local midnight (Soler et al., 2021) and up to $0.1 \text{ km}^{-2} \text{ night}^{-1}$ (Husbjerg et al., 2022). Previous studies modeled photon scattering and absorption emissions to estimate the depths of the blue corona sources. They assumed cloud microphysical parameters, such as a mean particle radius of 10–20 μm and densities of $1\text{--}2.5 \times 10^8 \text{ m}^{-3}$, resulting in photon mean free paths of 1–20 m (Heumesser et al., 2021; Husbjerg et al., 2022; Li et al., 2021, 2022b; Luque et al., 2020; Soler et al., 2020). The results indicated that blue corona discharges are expected to occur between cloud tops and the interior to a depth of $\leq 4 \text{ km}$ in the tropics and $\leq 1 \text{ km}$ at mid- and higher latitudes, or globally within clouds at depths $\leq 8 \text{ km}$ according to Husbjerg et al. (2022). We know they are generated in both the growing and collapsing stages of the convective cells (Dimitriadou et al., 2022) and favor stronger convection and higher cloud tops than normal lightning (Husbjerg et al., 2022). However, the conditions in the clouds that generate them are not well understood.

Here we present an analysis of 92 blue corona discharges observed within the cloud cells of cyclone Fani, along with independent measurements of the cloud-top microphysics of one of the parent thunderstorm cells taken 12 min later by the Cloud-Aerosol Lidar and Infrared Pathfinder Satellite Observation (CALIPSO). We analyzed the depth of the optical pulses observed by ASIM using the first-ever measured cloud-top microphysics related to blue corona discharges from CALIPSO and the ground-based electromagnetic (EM) measurements of NBEs from the Earth Networks Total Lightning Network (ENTLN) (Zhu et al., 2017, 2022). We first present the instruments and observations. Then, we apply a light-scattering model by considering the cloud properties to derive the depth of the discharges and compare them with the radio-derived altitudes. Finally, we discuss the relationship between the blue corona discharges, the NBEs and the lightning activity.

2. Instruments and Observations

On 26 April 2019, a tropical depression in the southern region of the Bay of Bengal intensified into Cyclone Fani. As Fani moved northward, it developed into a category 5 cyclone on 2 May with wind speed up to 250 km/hr. It was the most severe cyclone in the Bay of Bengal since 1999, killing 81 people and causing damage of approximately 8.1 billion US dollars at landfall in Bangladesh and India (Chauhan et al., 2021; Zhao et al., 2020).

ASIM passed over Fani on 30 April 2019, when it was a category 3 cyclone. Its nadir-pointing instruments include three photometers that sample at 100 kHz and two cameras that image at 12 frames per second. The photometers measure part of the Lyman–Birge–Hopfield (LBH) band of N_2 in the UV band at 180–230 nm, a line of the second positive system of N_2 at 337 nm (blue) with 3 nm bandwidth, and an atomic oxygen line at 777.4 nm (red) with 5 nm bandwidth. The cameras measure in the blue and red bands of the two photometers with $1,000 \times 1,000$ pixel resolution. The cameras' square Field-Of-View (FOV) was 400×400 km² on the ground, and the photometers' circular FOV had a radius of ~ 283 km, as shown in Figure 1a. The figure also shows the cloud-Top Blackbody Brightness (TBB) temperature derived from the Himawari-8 satellite data (Bessho et al., 2016) at 20:10:00 UTC. During its 1-min overpass from 20:10:55 to 20:12:05 UTC, ASIM detected 92 blue corona discharges from two convective cells in the outer rainband region of the cyclone system (marked by α), about 200 km from the cyclone center. Although the cells have independent storm structures, they are likely affected by the cyclone environment. However, due to insufficient measurements of the cyclone system's thermodynamic structure, we cannot explore if these convective cells can be considered part of the cyclone or an adjacent but independent system.

The smaller region marked with β in Figure 1a, with a size of about 50 km², was observed by CALIPSO from 20:23:58 to 20:24:14 UTC, about 12 min after ASIM. The CALIPSO lidar is oriented toward the nadir. It measures the vertical distribution of cloud hydrometeor properties with a footprint of about 90 m (Delanoë & Hogan, 2010; Gryspeerdt et al., 2018; Z. Liu et al., 2009; Sourdeval et al., 2018). The black stars are the sensor locations of the ENTLN that measure the EM radiation from lightning discharges and NBEs.

ASIM has an absolute timing uncertainty of tens of milliseconds since the data are not time tagged by a dedicated Global Positioning System (GPS). The absolute time of ASIM is provided from the ISS GPS receiver. It is passed to the payloads through the ISS networks and the Data Handling and Power Unit (DHPU) of ASIM. Because the central time process in the DHPU is clocked at 60 Hz and the time input from the ISS is not prioritized, the timestamp gets an uncertainty of up to two clock cycles, that is, $2 \cdot 1/60 = 33.333$ ms (Heumesser, 2021). We can improve its accuracy to the millisecond level by cross-correlating the times of 777.4 nm-pulses detected during the overflight by the Lightning Imaging Sensor (LIS) collocated with ASIM on the ISS. To obtain a “light” curve for LIS, we integrated the LIS group radiance by binning it over 2 ms and then cross-correlated it with the peak time of the 777-nm photometer pulse to determine the time shift of ASIM (Bitzer et al., 2021; Heumesser et al., 2021). Based on our analysis, we found that the systematic time shift of ASIM with respect to LIS, $\Delta t = T_{LIS} - T_{ASIM}$, was approximately 1.4 ± 1.1 ms (see Figure S1 in Supporting Information S1). Note that Δt could be affected by the binning boundaries for the LIS data, but it stayed under 1 ms (half of 2 ms).

Previous studies suggest that ASIM image data projected to cloud-top altitudes have an uncertainty of less than 10 km in latitude and longitude (Husbjerg et al., 2022; Neubert et al., 2021). In our study, we estimated the locations of the blue corona discharges by projecting the 337 nm camera images or camera metadata (if the camera images were not available, see Table S1 in Supporting Information S1) to an altitude of 16 km, based on the World Geodetic System (International Civil Aviation Organization, 2002). The altitude is an estimation of the average altitude of the blue corona discharges inferred from the Cloud Top Height (CTH) obtained from CALIPSO and the depths calculated using a light-scattering model (see Section 3.2 for more details). The accuracy of the CTH from CALIPSO has been previously estimated to be within 1 km (Di Michele et al., 2013; C.-Y. Liu et al., 2020). Considering ASIM's observation geometry, an uncertainty of 1 km in the CTH measurement corresponds to a location shift of approximately 0.5 km in the projection of the camera image. The uncertainty of the location is relatively small compared to the size of the cloud, and therefore, it is not considered to impact our conclusions.

The Convective Available Potential Energy (CAPE) from ERA5 hourly re-analysis data at 20:00:00 UTC is shown in Figure 1b. ERA5, known as the European Center for Medium-Range Weather Forecasts Reanalysis version 5, provides hourly estimates of atmospheric, land and oceanic climate variables on a 30 km horizontal grid, and resolves the atmosphere into 137 levels from the surface to 80 km altitude (Hersbach et al., 2020). We

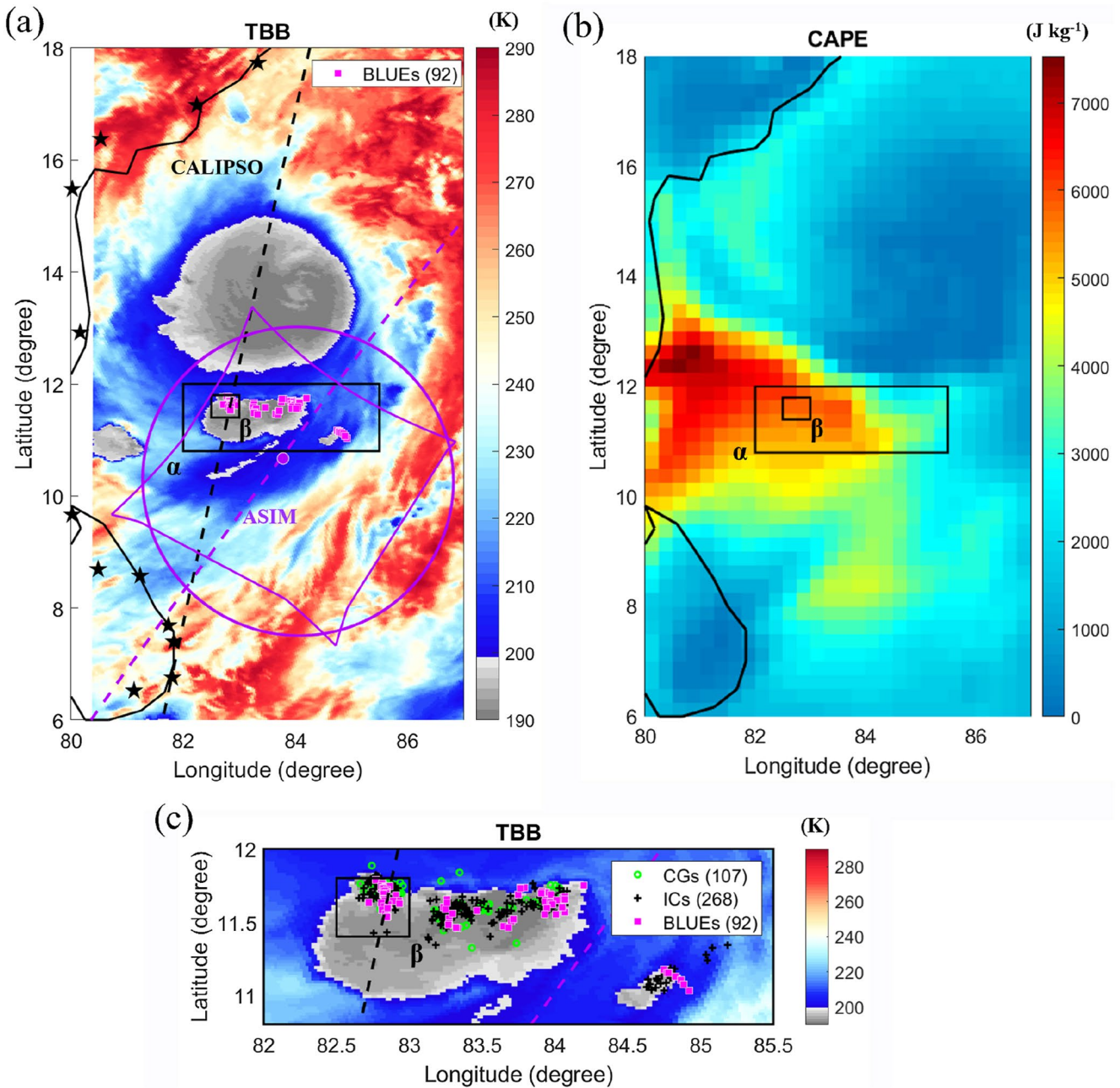


Figure 1. An overview of cyclone Fani. (a) The Top Blackbody Brightness (TBB) temperature provided by the Himawari-8 satellite at 20:10:00 UTC with the footprints of Atmosphere-Space Interactions Monitor (ASIM) moving eastwards and Cloud-Aerosol Lidar and Infrared Pathfinder Satellite Observation (CALIPSO) moving westwards. Black stars mark the locations of the ENTNLN network stations. The convective clouds with blue corona activity are in region α , and the smaller region sampled by CALIPSO is region β . (b) Convective Available Potential Energy (CAPE) based on ERA5 hourly reanalysis data at 20:00:00 UTC. (c) Region α with the blue corona discharges, Cloud-to-Ground (CG) and Intracloud (IC) lightning activity superimposed. The fields of view of both photometer (purple circle) and camera (purple square) of ASIM corresponding to the overpass time at 20:11:20 UTC (purple solid dot) are shown in (a).

saw the blue corona discharges in regions where CAPE reached about $6,000 \text{ J kg}^{-1}$, which, according to Husbjerg et al. (2022), was one of the highest values associated with blue corona discharges during the past 3 years of ASIM observations. The cloud cells formed as air was carried by cyclone winds from mainland India over the Bay of Bengal. The magnitude of the 200–850 hPa vertical wind shear at the center of region β , $\sim 20 \text{ m s}^{-1}$ (not shown here), was typical for severe convective storms (Pucik et al., 2021).

Figure 1c shows a zoom of the corona-active α region. ASIM and CALIPSO passed over the smaller β region within 12 min of each other. The blue corona discharge locations (pink squares) are shown with Cloud-to-Ground (CG) (green circles) and Intracloud (IC) lightning (black crosses) detected by ENTLN during the time of ASIM observations.

The statistical significance of the optical pulses detected by the three photometers for 92 blue corona discharges was estimated by calculating the mean (μ) and standard deviation (σ) for the binned average of 40 data samples (0.4 ms), as described by Li et al. (2021). Pulses for which the blue peaks were above 5σ were accepted as blue corona discharges. Their rise times ranged from 10 to 370 μ s and their durations from 90 to 7,670 μ s (see Table S1 in Supporting Information S1). The UV emissions coinciding with the blue peaks were negligible and below the 1σ level. Of the 92 cases, 89 had red peaks below 1σ . The remaining 3 cases were associated with weak red emissions below 3σ (see Figures A2–A4 in Appendix A), with blue (337 nm)/red (777.4 nm) ratios of 5.0, 8.5 and 8.8. They were not detected in the red camera nor by LIS. Two examples of blue corona discharges, one with negligible and one with weak red emissions, are shown in Figure 2 (see the statistical significance of these signals in Figures A1 and A2 in Appendix A).

3. Analysis and Results

3.1. Cloud Microphysical Properties Detected by CALIPSO

The CALIPSO lidar measures the properties of optically thin clouds (optical depth between 0.3 and 3) with a sensitivity that allows the detection of small ice crystals (effective diameter $D < 15 \mu$ m) in cloud tops that generally are missed by meteorological radars (Hagihara et al., 2014; Mitchell et al., 2018; Winker et al., 2010). In our analysis, we focus on the β region over which CALIPSO passed ~ 12 min after ASIM. During this time, the number of lightning events in the β region decreased from 63 min^{-1} to 51 min^{-1} and the average TBB temperature varied by less than 1 K, suggesting that only minor changes happened in the cloud (see Appendix B for more details). Thus we assume that the CALIPSO measurements were applicable during the occurrence of blue corona discharges. The measurements from CALIPSO represent an improvement over the assumed cloud microphysical properties in previous studies analyzing the effects of cloud scattering on the pulse shapes of optical blue corona discharges.

Figure 3a shows the 532 nm total backscatter coefficient along the trajectory of CALIPSO in the region α , and Figure 3b gives the CTH derived from these measurements. The tropopause height in the CALIPSO data product is provided by NASA's Global Modeling and Assimilation Office (Lidar Level 1 V4.10 Data Product Descriptions, 2016). Time increases toward the right along the horizontal axis, indicating the latitude and longitude of the satellite. The main cloud reached above 17 km from 11.76° to 11.50° latitude, which was likely where the main updraft occurred. The cloud protruded above the tropopause, with a gullwing-shaped cirrus layer of ice crystals pumped into the lower stratosphere (O'Neill et al., 2021; Wang et al., 2016) and carried from the region by wind shear near the cloud top.

Figures 3c–3f show a selection of microphysical properties based on the raDAR/liDAR (DARDAR) cloud products (Delanoë & Hogan, 2010): the categorization (c), particle radius (d), ice crystal number density (e) and photon mean free path (f). These products are normally found with a variational method and, in the case of the ice crystal number density, by combining lidar and CloudSat radar measurements (Delanoë & Hogan, 2010; Gryspeerdt et al., 2018; Sourdeval et al., 2018). Because CloudSat data were unavailable, we determined the ice crystal number density (e) from the ice water content following Sourdeval et al. (2018), assuming crystal diameters are above 5 μ m.

Photon mean free path Λ is the average distance that a photon can travel before being scattered or absorbed by the cloud particles. The amount of scattering and absorption depends on the density and size of the particles, as well as the wavelength of the light. The shorter the photon mean free path, the more scattering and absorption in the cloud. The mean free path is estimated through:

$$\frac{1}{\Lambda} = \int_0^{\infty} \frac{\pi}{4} D^2 Q_{ext} N(D) dD, \quad (1)$$

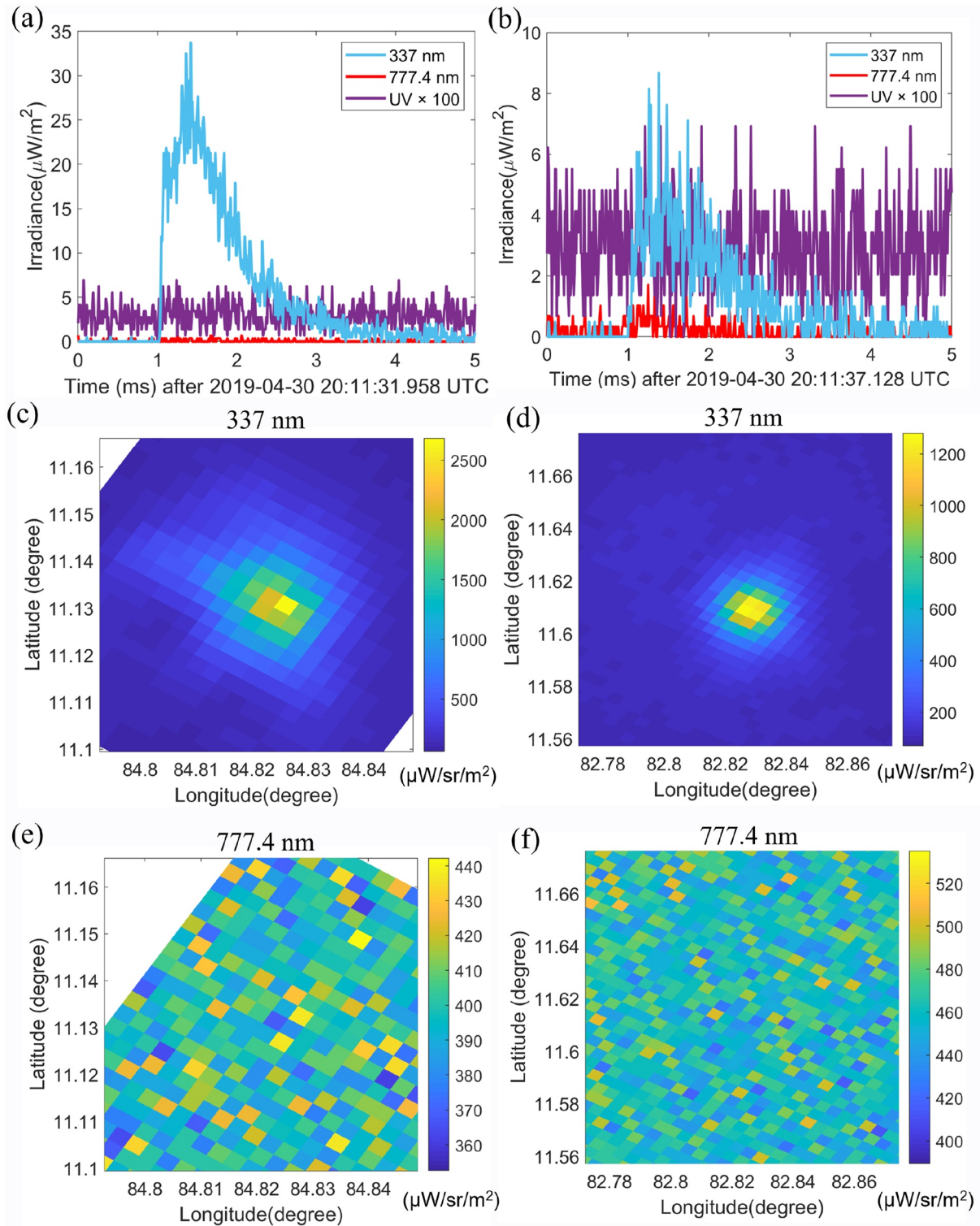


Figure 2. Two examples of blue corona discharges with negligible (a, c, e) and weak red emissions (b, d, f). (a, b) Three photometer signals (blue: 337 nm, red: 777.4 nm and purple: 180–230 nm (ultraviolet [UV]) $\times 100$), (c, d) the 337 nm camera images and (e, f) the 777.4 nm camera images.

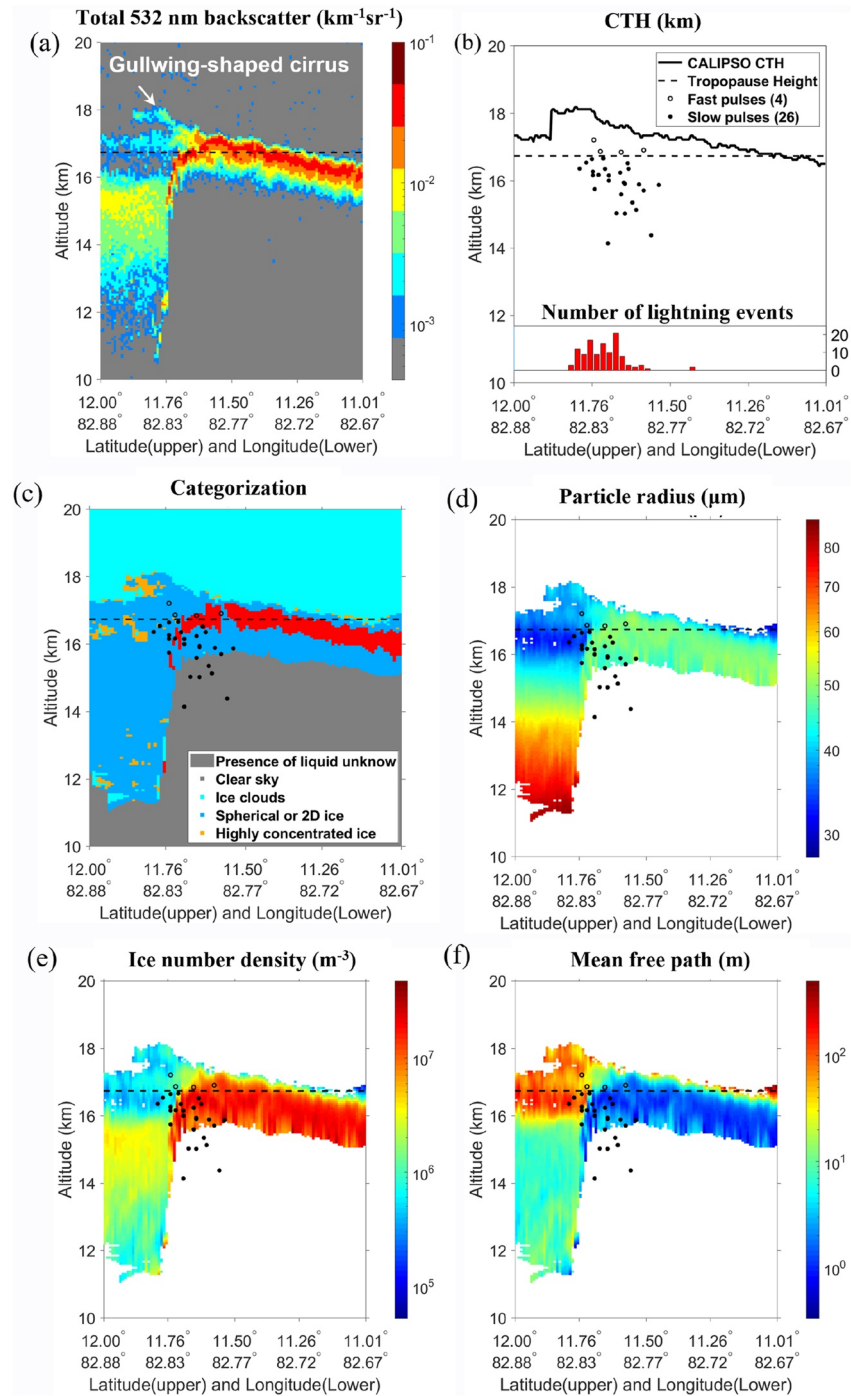


Figure 3. The Cloud-Aerosol Lidar and Infrared Pathfinder Satellite Observation (CALIPSO) measurements along the trajectory in region α with the blue corona discharges in region β . Time increases along the horizontal axis toward the right; the black dashed line marks the tropopause height. (a) A cross-section of the 532 nm lidar backscattering coefficient profile with a gullwing-shaped cirrus in the lower stratosphere, (b) The Cloud Top Height (CTH) measured by CALIPSO with the depths of the blue corona discharges in region β inferred from the optical pulses. The fast and slow pulses are shown in empty and filled circles, respectively. The inserted histogram shows Earth Networks Total Lightning Network lightning activity in region β binned with 0.02° (approximately 2 km) in latitude along the CALIPSO trajectory during the Atmosphere-Space Interactions Monitor overpass. The remaining panels are based on DARDAR cloud products including (c) categorization, (d) particle radius, (e) ice crystal number density, and (f) photon mean free path.

where D is the particle diameter; $Q_{ext} \approx 2$, is the extinction efficiency in the 337 nm band using Mie theory; $N(D)$ is the distribution function of the particle diameters.

Figures 3c–3f show that the main cloud on the left (11.76° – 12°) below the tropopause had relatively low number density. A gull-wing-shaped layer of cirrus cloud extended from the highest cloud top. The cloud tops on the right (11° – 11.76°) contained highly concentrated ice with a photon mean free path ~ 3 m. DARDAR Cloud products identify different types of attenuating 532 nm backscatter layers and classify them according to temperature and parameters from the radar and lidar masks (more details on this categorization process can be found in Ceccaldi et al. (2013)).

Note that the accuracy and reliability of CALIPSO measurements decrease as the cloud optical depth (COD) increases. CALIPSO cannot penetrate relatively thick clouds with COD between 3 and 5 (Z. Liu et al., 2005). As illustrated in Figure 3, CALIPSO provided information at altitudes above 11 km in regions larger than 11.76° latitude, and above 15 km below 11.76° latitude as indicated by the label “Presence of liquid unknown” in Figure 3c.

By utilizing CALIPSO's measurements to estimate the photon mean free path, mean particle size, and density, we calculated the cloud scattering and absorption of the optical emissions from blue corona discharges without making assumptions. Figures 3d and 3e show that most blue corona discharges were associated with ice particles with a radius of ~ 50 μm and a number density of $\sim 2 \times 10^7$ m^{-3} at an average altitude of approximately 16 km. Using Equation 1, the photon mean free path Λ was calculated to be 3 m. Previous studies modeled the scattering and absorption emissions from blue corona discharges by assuming mean particle radius of 10–20 μm and densities of 1 – 2.5×10^8 m^{-3} , resulting in photon mean free paths of 1–20 m (Heumesser et al., 2021; Husbjerg et al., 2022; Li et al., 2021, 2022b; Luque et al., 2020; Soler et al., 2020). Our data-based results support the assumptions used in previous works.

We spatially grouped the lightning flashes detected by ENTLN in the region β during the ASIM overpass from 20:10:55 to 20:12:05 UTC. The bins are 0.02° in latitude (approximately 2 km). As shown in Figure 3b, lightning and blue corona discharges were observed in the overshooting top region, indicating a strong updraft that lifted ice particles into the stratosphere and formed the gullwing-shaped cirrus. Interestingly, CALIPSO measured a high concentration of large ice particles at latitudes between 11.0° and 11.5° , but no lightning or blue corona discharge were detected in this region. Note that the global stroke detection efficiency of ENTLN is approximately 97%; however, it may vary in regions with limited sensor coverage (Zhu et al., 2022). We estimated the ENTLN detection efficiency in the region shown in Figure 1 by comparing it with LIS observations. The results indicated that ENTLN had a detection efficiency of around 50% for both IC and CG flashes across the entire region during the ASIM overpass period. Nevertheless, it is expected that the detection efficiency for the more intense NBEs will be higher.

3.2. Estimation of Source Depth

As photons travel through a cloud, they can be scattered or absorbed by the particles inside the cloud. The time it takes for the photons to reach the detector is determined by the path of the scattering and absorption by cloud droplets and ice crystals (Light et al., 2001; Luque et al., 2020; Thomson & Krider, 1982). Therefore, photons that originate from deeper within the cloud with more scattering and absorption will on average take longer to reach the detector, resulting in a longer rise time for the corresponding optical pulse.

In our study, we estimate the depth relative to the cloud top of the blue corona discharges from the 337 nm photometer pulses detected by ASIM. We only focused on the blue corona discharges in the β region that ASIM and CALIPSO both passed over. We assumed that the particle radius and number density determined by CALIPSO represent the cloud microphysical properties relevant to the blue corona discharges in β region. We used the mean free path that we previously estimated, $\Lambda = 3$ m, based on the first-hitting-time (FHT) model (Li et al., 2023; Soler et al., 2020) in Equation 2, and fitted the parameters A and L to the optical pulses, with L being the depth of the blue corona discharges in the cloud.

The FHT model assumes the discharges are instantaneous and localized point sources inside a homogeneous, isotropic scattering cloud (Luque et al., 2020; Soler et al., 2020). For the wavelength of our interest (337 nm), we only considered Mie scattering and absorption by cloud particles because they dominate over Rayleigh scattering and atmospheric absorption, respectively. The collision rate is $\nu = c/\Lambda$, where c is the speed of light and

the photon mean free path Λ is assumed constant in the cloud. Mie scattering and absorption at 337 nm are characterized by the scattering asymmetry parameter $g \approx 0.87$; the respective extinction coefficient $Q_{ext} \approx 2.015$; and the single-scattering albedo $\omega_0 \approx 1 - 10^{-7}$, which describes the probability that a photon is not absorbed in a scattering event. The photon flux has the following expression, which is valid for $t > 0$, with the time origin defined as the moment of light emission (Luque et al., 2020):

$$F(t) = A \frac{e^{-t/\tau_A - \tau_D/t}}{\sqrt{\pi \tau_D}} (t/\tau_D)^{-3/2}, t > 0 \quad (2)$$

where A is the number of photons emitted by the source; $\tau_A = 1/(\nu(1 - \omega_0))$ is the photon absorption time; and $\tau_D = L^2/(4D)$ is the diffusion time corresponding to the distance L to the source location. The diffusion coefficient is $D = c^2/(3\nu(1 - \omega_0g))$.

The FHT model only describes single pulses with clear impulsive signals, so we created two criteria to filter out more complex events involving multiple pulses (Li et al., 2022b). The analyzed optical pulses had to have a determination coefficient (R^2) greater than 0.6 and a Pearson correlation coefficient (ρ) lower than 0.5.

Based on the 10 μ s temporal resolution of the photometer signals, we categorized the optical pulses as fast if their rise time was $\leq 30 \mu$ s and slow if they were longer, following the method used in Husbjerg et al. (2022). In the β region sampled by CALIPSO, 30 out of 40 optical pulses were fitted using the FHT model. Among them, 4 were categorized as fast and 26 as slow. The source altitudes ($CTH - L$) inferred from these optical pulses are presented in Figure 3 with empty and filled circles. Figures 4a and 4b shows two examples of fast and slow discharges along with the fitting results based on the FHT model.

3.3. Blue Corona Discharges With NBEs

To verify if the blue corona discharges are NBEs, we searched for NBEs in the ENTLN radio signals with a machine-learning algorithm proposed by Zhu et al. (2021). To make the identification more robust, and to allow us to estimate the source altitudes, we required the NBEs to last for 5–50 μ s and have clear ground waves and reflected sky waves. Based on the atmospheric electricity sign convention, the polarity of NBEs was defined by the polarity of the first half cycle of its ENTLN radio waveform. Figure 4 shows two examples of both fast and slow discharges associated with $-$ NBE and $+$ NBE observed by different ENTLN sensors located at different observation distances, where the ground wave is marked “G” and the reflected sky waves are marked “S.”

As discussed above, we corrected the time uncertainty of ASIM by cross-correlating with LIS data. Using this time correction, we first adjusted the detection times of the blue corona discharges to their source times based on the source locations. We then identified the corresponding radio signal of NBEs by considering the effect of propagation delay from the source to the detector, only accepting a match if the radio signal peak was within 1 ms before the optical peak.

With this procedure, we found 15 out of 92 blue corona discharges were identified as NBEs, including 12 $+$ NBEs and 3 $-$ NBEs. The number of matched blue corona discharges and NBEs may have been underestimated due to the fact that ENTLN only saves radio signals in proximity to their detected peaks. In addition, our analysis only accepted short radio pulses lasting for a few to tens of microseconds, with clear ground waves and reflected sky waves, as NBE events (see Figure 4). It is possible that ENTLN captured only a few data points of weaker NBE pulses, which were excluded from our statistics. However, the low number of matched events suggests that optical measurements from the ISS may be more sensitive than the current radio observations for detection of blue corona discharges/NBEs when these occur in the upper regions of clouds. It is also possible that some of the discharges may be related to streamer activity at the onset of lightning leader formation (Kostinskiy et al., 2020; Li et al., 2022b, 2023; López et al., 2022; Lyu et al., 2019; Marshall et al., 2019; Rison et al., 2016), or that the radio signals are weak due to their horizontal orientation (Li et al., 2022b, 2023).

Previous studies indicated (F. Liu et al., 2021a; Soler et al., 2020) that $+$ NBEs were more likely to be associated with blue corona discharges exhibiting longer rise times (slow corona discharge) deep within the clouds, while $-$ NBEs were connected to blue corona discharges with short rise times (fast corona discharge) at the cloud tops. Out of the 12 $+$ NBEs, one matched a fast corona discharge, and 11 matched slow corona discharges. Among the

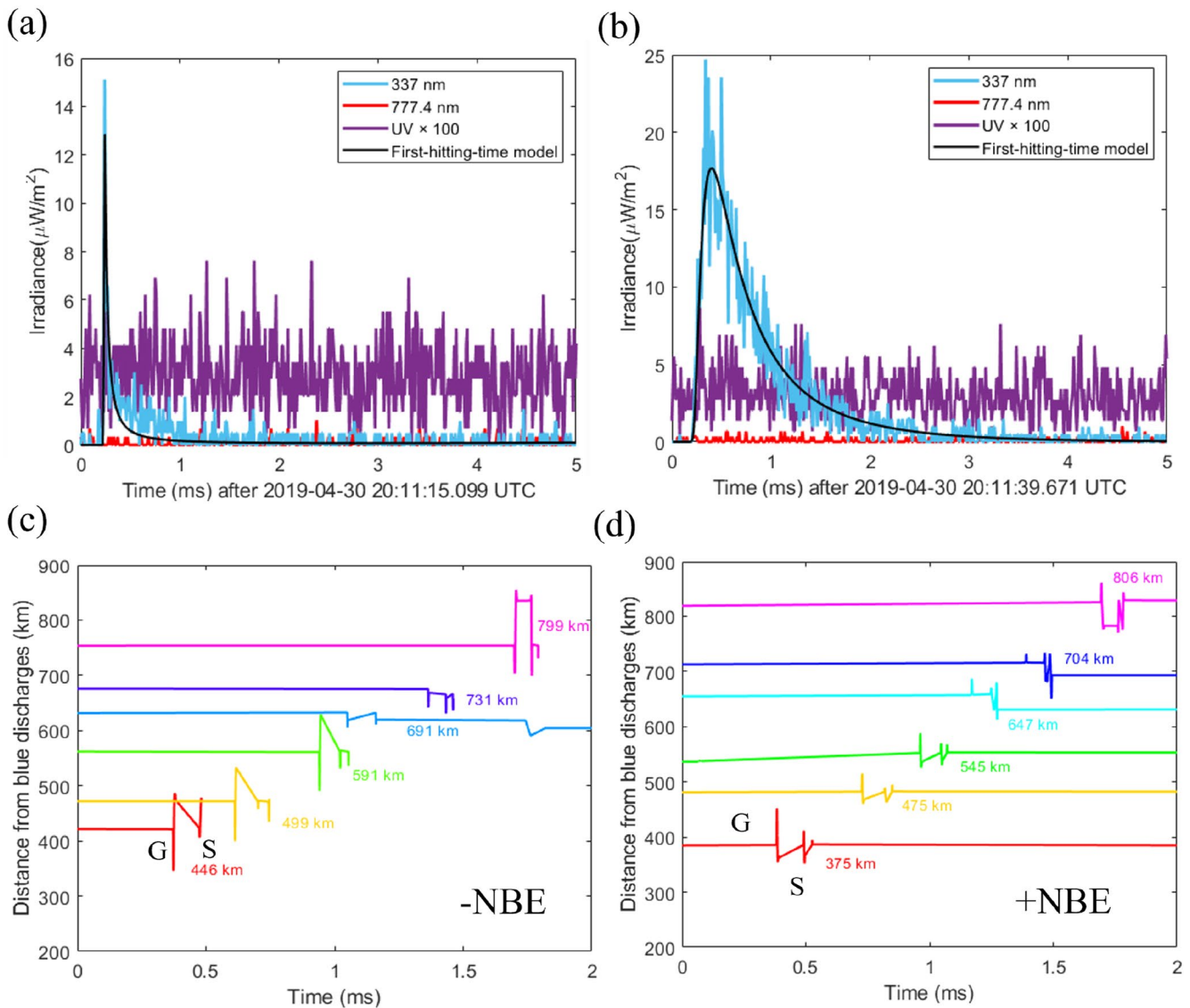


Figure 4. Two example of blue corona discharges (fast discharge (a) and slow discharge (b)) associated with $-NBE$ (c) and $+NBE$ (d) observed by different Earth Networks Total Lightning Network sensors located at different observation distances. The ground wave and the reflected sky waves are marked as “G” and “S” in (c) and (d).

3 $-NBEs$, one was linked to a fast corona discharge, and two were connected to slow corona discharges. However, the number of events in the Fani storm is too limited to allow any generalization.

To compare the source altitudes derived from both the optical and radio bands, we estimated the altitudes of nine blue corona discharges that were identified as $NBEs$, using two different methods. One method was based on the optical measurements and the other used radio signals. For the optical band, the depth in the cloud, L , was found by fitting the photometer signal with the FHT model in Equation 2, using the photon mean free path $\Lambda = 3$ m, consistent with the CALIPSO measurements. Figure 5a shows the height estimated from the optical pulses $H_{Optical} = CTH - L$, where CTH was derived from CALIPSO measurements. The altitude H_{Radio} from the radio signal (see Figure 5b) was estimated using the simplified ray-propagation method developed by Smith et al. (1999, 2004), based on the observation distances and the time differences between the ground wave and 1-hop sky waves. The two approaches are in agreement, as seen in Figure 5c, with a maximum deviation of 1 km for event 6.

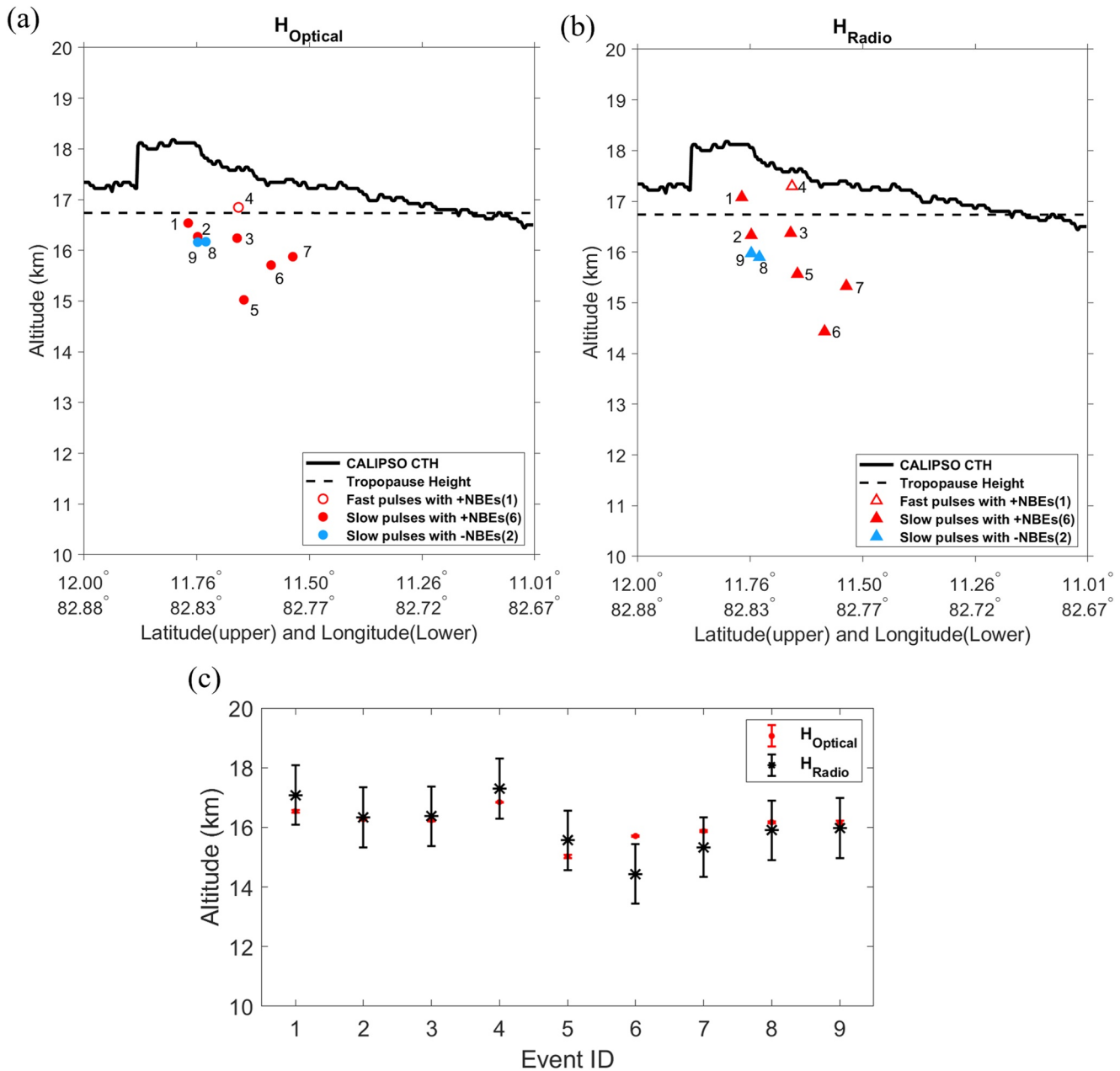


Figure 5. Comparison of the source altitudes estimated from the 9 blue corona discharges identified as Narrow Bipolar Events (NBEs) in region β . (a) The optical inferred altitudes of blue corona discharges ($H_{Optical}$). (b) The radio inferred altitudes of NBEs (H_{Radio}). The black solid curves in (a) and (b) mark the Cloud Top Height (CTH) measured by Cloud-Aerosol Lidar and Infrared Pathfinder Satellite Observation (CALIPSO) and the dashed line mark the tropopause height. (c) Comparison of the altitudes determined by the two methods. Error bars corresponding to both radio and optical method are shown on H_{Radio} and $H_{Optical}$.

According to Li et al. (2020), the H_{Radio} calculated using the simplified ray-propagation method, which assumes straight ray paths and ideal reflections between the ground and an effective (or virtual) ionospheric reflection height, had an uncertainty of approximately ± 1 km compared to the full-wave method. The full-wave method takes into account different frequency components that are reflected at different heights in the ionosphere. The uncertainty of $H_{Optical}$ was evaluated by taking the square root of the estimated variance of the fitting coefficient in the FHT model, which was found to be less than 0.06 km. Note that this represents a measure of the statistical uncertainty; the model uncertainty due to our ignorance about the precise cloud composition is harder to estimate, but likely much larger.

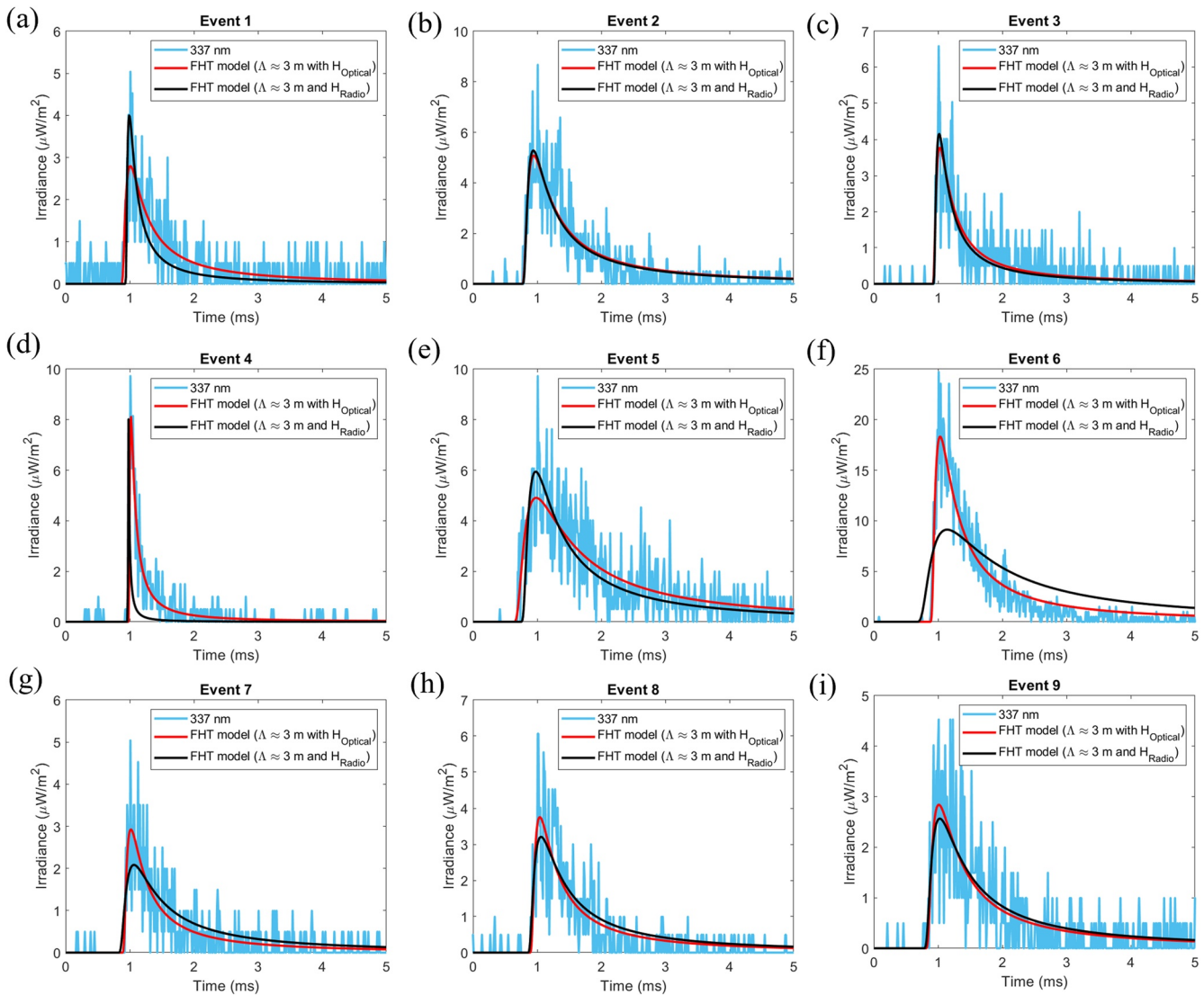


Figure 6. The 337 nm photometer signals of the 9 blue corona discharges with Narrow Bipolar Events in region β . The first-hitting-time (FHT) modeling results by using the altitudes derived from the optical and radio observations are superimposed. The photon mean free path is assumed $\Lambda = 3$ m for all the events.

Figure 6 displays a comparison of nine optical pulses in the β region between the observed 337-nm photometer signals and the FHT modeling results based on optical and radio derived heights with a photon mean free path of 3 m. To assess the uncertainty of the height estimated from the optical pulses $H_{Optical}$, we considered the altitude H_{Radio} derived from the radio band to be the “true” source altitude since the actual uncertainty of the optical method associated with the specific cloud microphysical features was challenging to quantify. We see that events 4 and 6 have poor radio fits with the coefficient of determination $R^2 < 0.2$. They are the shallowest and deepest events. The poor fit likely reflects the uncertainties in estimates of optical depths based on the FHT model. In the model, we assumed the photon mean free path to be homogeneous, but for sources that are located near the top or deep inside the cloud, the cloud composition may be more complex and inhomogeneous. If the assumed Λ is too small, the estimation of the optical depths will be higher than the actual sources in the cloud, which appears to be the case for event 4 in Figure 6d. Comparing Figures 5a and 6f, we see the photon mean free path, Λ , is likely higher than 3 m for the deepest event 6, due to the complex cloud microphysical features.

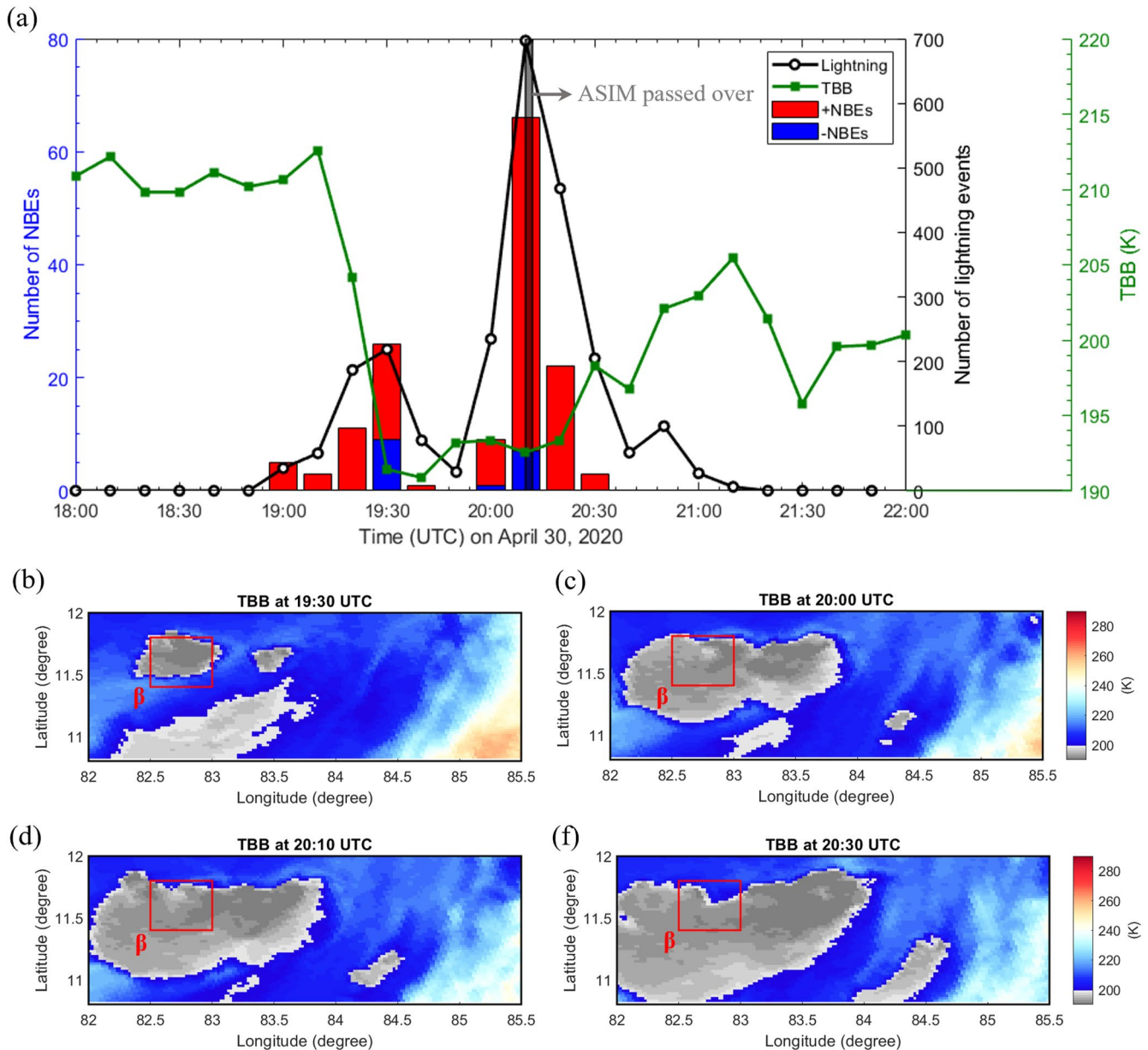


Figure 7. The time evolution of electrical activity. (a) Lightning and Narrow Bipolar Events (NBEs) in region β along with Top Blackbody Brightness (TBB) temperature at the center of region β . The time period of the 92 blue corona discharges detected by Atmosphere-Space Interactions Monitor (ASIM) is marked by the gray rectangle and (b–f) TBB temperature in region α at 19:30 UTC, 20:00 UTC, 20:10 UTC and 20:30 UTC.

3.4. Electrical Activity in Relation to the Phase of the Storm Cell

The blue corona discharges observed by ASIM represent a snapshot of the cell's electrical activity. To understand the development phase of the thunderstorm cell in which the discharges were generated, we analyzed the TBB temperature provided by the Himawari-8 satellite and ENTLN lightning data from 2 hr before and after ASIM overpass. Figure 7a shows the lightning, NBEs and the TBB temperature at the center of region β . Figures 7b–7d shows the TBB in the corona-active region α in Figure 1c, before, during, and after the ASIM overpass. A movie with all TBB images during the 4-hr period is included in Supporting Information S1 (Movie S1).

We see that the localized storm cell in region β started to develop around 19:00 UTC, where lightning and +NBE activity began. About 30 min later, the cloud top temperature dropped from 210.6 to 191.4 K until the cloud cell completely filled the β region. The number of lightning and +NBE event increased to a local maximum of

219 and 17, respectively, at 19:30 UTC, when $-$ NBEs were also detected. After a decline, the activity picked up again a few minutes before 20:00 UTC, reaching a higher maximum of lightning and $+$ NBE counts of 697 and 59, respectively, at 20:10 UTC when ASIM passed over. Finally, the activity decreased around 20:40 UTC. During the second surge, the TBB temperature in the center of region β gradually increased from 20:00:00 to 20:30:00 UTC because the cloud cell continued to expand and drifted out of the region toward the East, as shown in Figures 7c, 7d, and 7f. The overshooting cloud top with a TBB temperature of less than 190 K, lasting for more than 20 min, indicated that the blue corona discharges occurred in a convection region where a strong updraft lifted the high-density ice particles to altitudes in the lower stratosphere.

$+$ NBEs were found to correlate with an increase in lightning activity and a decrease in the TBB temperature, while $-$ NBEs and blue corona discharges appeared when the TBB temperature dropped below 190 K and lightning was maximized. The maximum lightning rate was about 70 per min around 20:10 UTC. The first increase in electrical activity was clearly connected to convection seen as the rapid development of the cloud cell. The second larger increase was likely due to the merging of two localized cloud cells: the one in region β and another centered at longitude $\sim 83.5^\circ$ (see Figure 7b), which led to a more complex development of the cloud tops.

4. Discussion

ASIM measured 92 blue corona discharges during ~ 70 s as it passed over the thunderstorm cells in the outer rainbands of tropical cyclone Fani. The data we present are unique because they include measurements of both the optical and EM radiation from the discharges and as well as the microphysics of the cloud tops, where most of the discharges are located. The measurements show that the blue corona discharges occur close to the strong updraft region just a few kilometers below the cloud top.

The blue corona discharge rate is about two-thirds of the rate reported in Chanrion et al. (2017), which was observed in the Bay of Bengal and in a similar phase of thunderstorm cell development, that is, close to the maximum occurrence of lightning. However, it is important to note that ASIM was only able to observe during its overpass time. Therefore, it is possible that blue corona discharges may have occurred before and/or after the ASIM observation period. Our results suggest that blue corona discharges might be commonly generated near the top of the convective cells, where they are observable from space.

Blue corona discharges had rise times ranging from 10 to 370 μ s and durations varying from 90 to 7,670 μ s. They had a compact shape with an illuminated cloud top area ranging from approximately 4 to 140 km^2 , with brightness from 180 to 7,600 $\mu\text{W}/\text{Sr}/\text{m}^2$. They occur near the cloud overshooting top region, with depths ranging from 0.4 to 3.5 km. Note that the estimation of the rise time and duration of blue corona discharges are heavily influenced by the waveshapes of the optical signals detected by ASIM, especially for the cases with large oscillations. Since ASIM observes the thunderstorm in a nadir direction, it is difficult to distinguish between different blue emissions. Some of the recorded fast blue discharges with short rise times may be related to *small blue starters* and *small blue jets* that occur close to the cloud top, partially outside the cloud (Edens, 2011; Wescott et al., 2001), or they may be *gnomes*, less than 1 km above the cloud top with uniform optical emissions and compact shape (Lyons et al., 2003). Other possibilities include cloud-top *pixies*, which appear on the overshooting tops along with the *gnomes* (Lyons et al., 2003), or kilometer-scale *surface blue discharges* or *blue glimpses* that appear to “dance” on the upper layer of the cloud (Chanrion et al., 2017). The slower blue discharges with longer rise times, located deeper inside the cloud, are more complex and may be related to “in-cloud streamer corona discharges” (Gordillo-Vázquez & Pérez-Invernón, 2021) or to the burst of streamers at the onset of lightning leader formation (Li et al., 2022b, 2023; López et al., 2022). However, leader initiation was not observed in our study.

Our observations indicate that blue corona discharges occurred in a convection region with CAPE reaching $\sim 6,000 \text{ J kg}^{-1}$, where a strong updraft lifted high-density ice particles to the lower stratosphere, which lasted for more than 20 min from 20:00 UTC to 20:20 UTC. This extended duration of overshooting cloud top may have facilitated conditions for blue corona discharges. Our findings that the blue corona discharges correlated with strong convection are consistent with previous studies (Chanrion et al., 2017; Dimitriadou et al., 2022; Husbjerg et al., 2022).

According to our observations, around 20% of the blue corona discharges detected were identified as NBEs by the ENTLN lightning detection network. It is generally agreed that $-$ NBEs are discharges between a cloud's upper positive charge layer and the negative screening layer attracted to the cloud tops (Smith et al., 1999, 2004;

Wu et al., 2012, 2014) and that +NBEs are located between the negative layer further down in the cloud and the upper positive layer (Karunarathne et al., 2015; Smith et al., 1999, 2004; Wu et al., 2012, 2014). Previous studies (F. Liu et al., 2021a) have suggested that blue corona discharges with longer rise times, occurring at deeper levels within the cloud, are associated with +NBEs, while –NBEs at the top of clouds are associated with blue corona discharges with short rise times (≤ 30 μ s). The trend is similar in the storm reported here, however, the conditions appear more complex. In the cases we report here, both polarities of NBEs were observed at similar altitudes, indicating that the organization of the charge layers were more complicated. This complexity could be due to the strong updraft and turbulence that lead to variations at smaller spatial scales in the charge layers near cloud tops, as suggested by earlier studies (Li et al., 2023; MacGorman et al., 2017; Stolzenburg et al., 1998; Stolzenburg & Marshall, 2009).

Our study indicated a close correlation between blue corona discharges and NBEs, which are characterized by a short duration (10–20 μ s) and a relatively compact spatial range of several hundred meters. The NBEs characteristics justify the assumptions used in our light-scattering FHT model: the blue corona discharge emission source is an instantaneous and localized point source. Under this assumption, the photometer signal's rise time depends on the photon propagation path rather than the source itself. Additionally, all the blue corona discharges have strong blue emission at 337 nm above 5σ level, with either no or weak red emission at 777.4 nm. The results further suggest that the primary source of blue corona discharge is dominated by streamers with fast speed, rather than leaders. Given this context, it is highly unlikely that the blue corona discharges are emitted from slow and continuous sources.

Our analysis was based on the cloud microphysical parameters measured from the CALIPSO lidar without making assumptions as the previous studies. The altitudes of nine blue corona discharges that were identified as NBEs are derived from both the optical and radio bands. It revealed that in six out of nine cases, the R^2 value was greater than 0.85, indicating a good agreement between the two methods and supporting our estimate of the photon mean free path as 3 m. However, in the shallowest and deepest cases, there was some discrepancy between the altitudes determined by the two methods, suggesting more complex cloud microphysical parameters. It is possible that the FHT model's simplification, including the homogeneous approximation for the cloud's microphysical parameters and the simplification of the source length, contributed to this uncertainty.

Appendix A: The Statistical Significance of Three Photometer Signals Detected by ASIM

In this appendix, we estimate the statistical significance of the three photometer signals (337 nm, 777.4 nm and 180–230 nm [UV]) for 92 blue corona discharges by calculating the mean μ and standard deviation σ for the binned average of 40 data samples (0.4 ms) based on the method proposed in Li et al. (2021). The 337 nm peaks for all the blue corona discharges were statistically significant above the σ level. Out of the 92 cases analyzed, 89 had red emissions below the 1σ level, indicating the absence of leader activity, as expected for corona streamer discharges. The remaining three cases were associated with weak red emissions below the 3σ level. Note that all of the UV emissions coinciding with the 337 nm peaks were below the 1σ level. The statistical significance of the three photometer signals for the blue corona discharges with negligible red emission corresponding to Figure 1a and another 3 cases (b–d) with weak red emissions are given in Figures A1–A4.

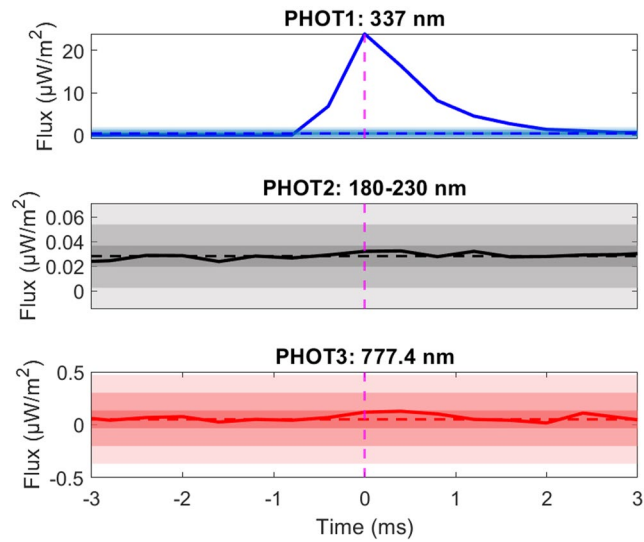


Figure A1. The statistical significance of the three photometer signals for the blue corona discharge with negligible red emission corresponding to Figure 1a. The horizontal dashed line is the mean of the background noises with the shaded bands indicating $\mu \pm \sigma$, $\mu \pm 3\sigma$, and $\mu \pm 5\sigma$.

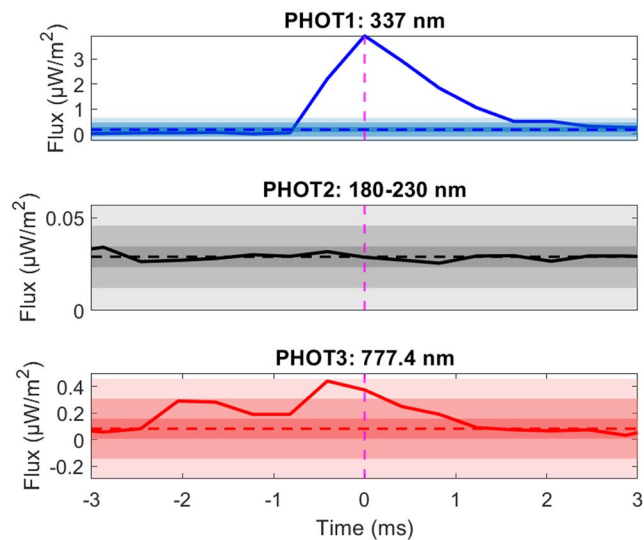


Figure A2. Similar to Figure A1, but for the first case of blue corona discharge with weak red emission corresponding to Figure 1b.

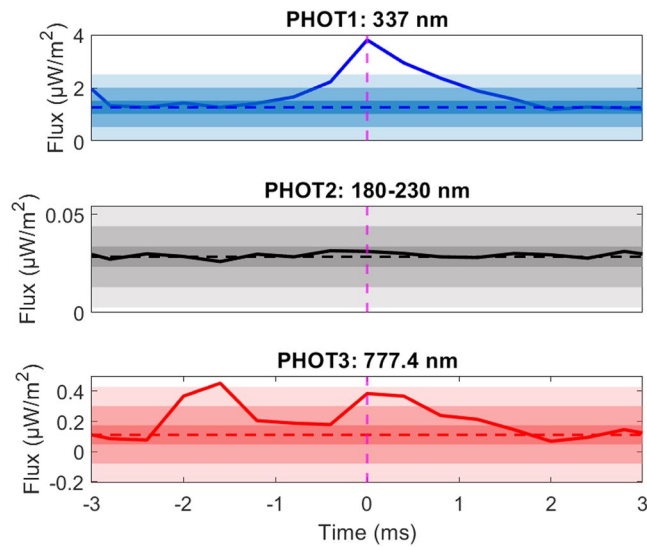


Figure A3. Similar to Figure A1, but for the second case of blue corona discharge with weak red emission.

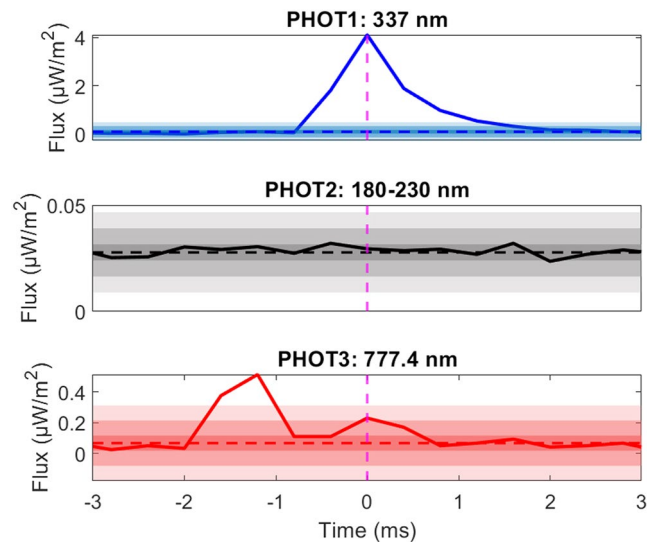


Figure A4. Similar to Figure A1, but for the third case of blue corona discharge with weak red emission.

Appendix B: The Statistical Significance of the Hydrometeor Composition Within a 12-min Time Difference Between ASIM and CALIPSO Observations

In this appendix, we estimate the statistical significance of the hydrometeor composition in the β region within a 12-min time difference between ASIM and CALIPSO observations. ASIM passed over the β region during the time period from 20:10:55 to 20:12:05 UTC, while the CALIPSO satellite passed over it subsequently, from 20:23:58 to 20:24:14 UTC. There is a time difference of approximately 12 min between the ASIM and CALIPSO observations.

The TBB temperature of the clouds, derived from Himawari-8 satellite data, is shown in Figure B1 along with the total number of lightning detected by ENTLN at 20:10:00 UTC and 20:20:00 UTC, respectively. It is important to note that during this time period, the total number of lightning decreased from 63–51 min^{-1} , while the average TBB temperature varied by less than 1 K and the cloud appeared to be relatively stable. Based on this observation,

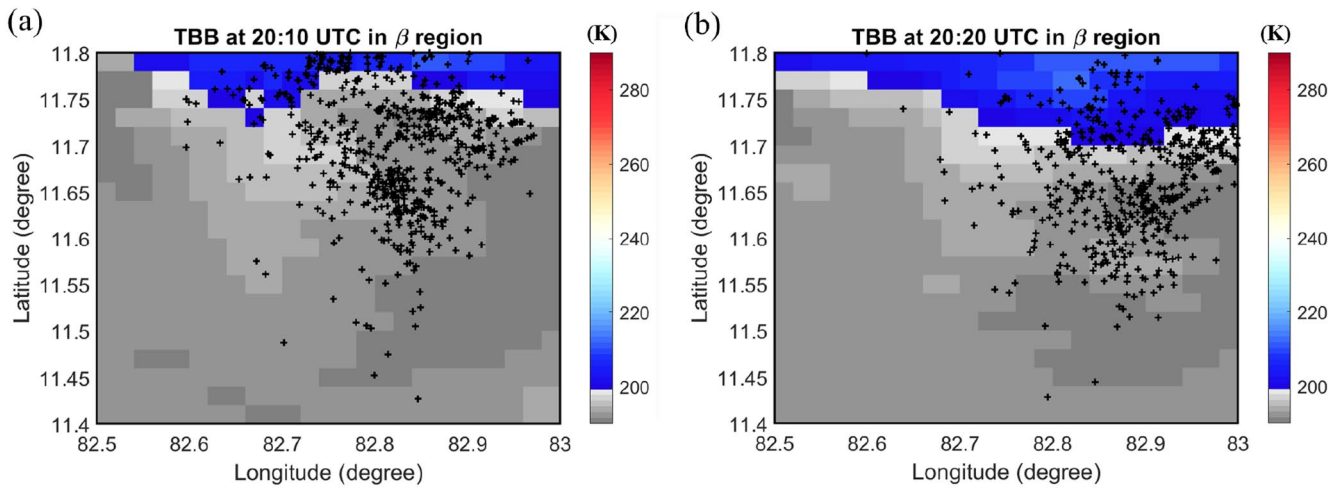


Figure B1. The Top Blackbody Brightness (TBB) temperature along with the lightning activity in the β region at 20:10:00 UTC (a) and 20:20:00 UTC (b).

we made the assumption that the hydrometeor composition measured by CALIPSO represented the cloud microphysical properties that were relevant to the blue corona discharges observed by ASIM 12 min earlier.

Data Availability Statement

The Modular Multispectral Imaging Array (MMIA) level 1 data is proprietary and not currently available for public release. Interested parties should direct their request to the ASIM Facility Science Team (FST). ASIM data request can be submitted through: <https://asdc.space.dtu.dk> by sending a message to the electronic address asdc@space.dtu.dk. The Himawari-8 gridded products are public to the registered users and supplied by the P-Tree System, Japan Aerospace Exploration Agency (JAXA)/Earth Observation Research Center (EORC) (<https://www.eorc.jaxa.jp/ptree/>). Earth Networks Total Lightning Network (ENTLN) products can be obtained from <https://www.earthnetworks.com/why-us/networks/lightning/> by contacting Earth Networks team through info@earthnetworks.com. The raDAR/lidAR (DARDAR) cloud products are public to the registered users at <https://www.icare.univ-lille.fr/dardar/overview-dardar-nice/>. CALIPSO data products are public to the registered users at <https://www.calipso.larc.nasa.gov/>. ERA5 hourly reanalysis data are public to the registered users, for the single level data can be found at <https://cds.climate.copernicus.eu/cdsapp#!/dataset/reanalysis-era5-single-levels?tab=overview>, for the pressure levels data can be obtained at <https://cds.climate.copernicus.eu/cdsapp#!/dataset/reanalysis-era5-pressure-levels?tab=overview>. NRT Lightning Imaging Sensor (LIS) on International Space Station (ISS) Science Data V2 is public to the registered users and is available at https://search.earthdata.nasa.gov/search?q=isslis_v2_nrt.

Acknowledgments

The authors thank Dr. Francisco C. Parra-Rojas and other two anonymous reviewers for their valuable comments and suggestions, which has greatly improved the paper. The authors would like to thank Dr. Carol Anne Oxborrow at Technical University of Denmark for her generous assistance in reviewing and refining the English language and grammar aspects of this work. This work was supported by Independent Research Fund Denmark (Danmarks Frie Forskningsfond) under Grant agreement 1026-00420B. The project has received funding from the European Union's Horizon 2020 research and innovation program under the Marie Skłodowska-Curie Grant agreement SAINT 722337. ASIM is a mission of the European Space Agency (ESA) and is funded by ESA and by national grants of Denmark, Norway and Spain. The ASIM Science Data Center is supported by ESA PRODEX contracts C 4000115884 (DTU) and 4000123438 (Bergen).

References

- Bai, X., Füllekrug, M., Chanrion, O., Soula, S., Peverell, A., Mashao, D., et al. (2023). Height determination of a blue discharge observed by ASIM/MMIA on the International Space Station. *Journal of Geophysical Research: Atmospheres*, *128*(7), e2022JD037460. <https://doi.org/10.1029/2022JD037460>
- Bessho, K., Date, K., Hayashi, M., Ikeda, A., Imai, T., Inoue, H., et al. (2016). An introduction to Himawari-8/9—Japan's new-generation geostationary meteorological satellites. *Journal of the Meteorological Society of Japan. Series II*, *94*(2), 151–183. <https://doi.org/10.2151/jmsj.2016-009>
- Bitzer, P. M., Walker, T. D., Lang, T. J., Gatlin, P. N., Chanrion, O., Neubert, T., et al. (2021). Multifrequency optical observations of lightning with ISS-LIS and ASIM. In *AGU fall meeting 2021*.
- Blakeslee, R. J., Lang, T. J., Koshak, W. J., Buechler, D., Gatlin, P., Mach, D. M., et al. (2020). Three years of the lightning imaging sensor onboard the International Space Station: Expanded global coverage and enhanced applications. *Journal of Geophysical Research: Atmospheres*, *125*(16), e2020JD032918. <https://doi.org/10.1029/2020JD032918>
- Ceccaldi, M., Delanoë, J., Hogan, R. J., Pounder, N. L., Protat, A., & Pelon, J. (2013). From CloudSat-CALIPSO to EarthCare: Evolution of the DARDAR cloud classification and its comparison to airborne radar-lidar observations. *Journal of Geophysical Research: Atmospheres*, *118*(14), 7962–7981. <https://doi.org/10.1002/jgrd.50579>
- Chanrion, O., Neubert, T., Mogensen, A., Yair, Y., Stendel, M., Singh, R., & Siingh, D. (2017). Profuse activity of blue electrical discharges at the tops of thunderstorms. *Geophysical Research Letters*, *44*(1), 496–503. <https://doi.org/10.1002/2016GL071311>

- Chanrion, O., Neubert, T., Rasmussen, I. L., Stoltze, C., Tcherniak, D., Jessen, N. C., et al. (2019). The Modular Multispectral Imaging Array (MMIA) of the ASIM payload on the international space station. *Space Science Reviews*, 215(4), 1–25. <https://doi.org/10.1007/s11214-019-0593-y>
- Chauhan, A., Singh, R. P., Dash, P., & Kumar, R. (2021). Impact of tropical cyclone “Fani” on land, ocean, atmospheric and meteorological parameters. *Marine Pollution Bulletin*, 162, 111844. <https://doi.org/10.1016/j.marpolbul.2020.111844>
- Chou, J. K., Hsu, R.-R., Su, H.-T., Chen, A. B.-C., Kuo, C.-L., Huang, S.-M., et al. (2018). ISUAL-observed blue luminous events: The Associated Sferics. *Journal of Geophysical Research: Space Physics*, 123(4), 3063–3077. <https://doi.org/10.1002/2017JA024793>
- Christian, H. J., Blakeslee, R. J., & Goodman, S. J. (1989). The detection of lightning from geostationary orbit. *Journal of Geophysical Research*, 94(D11), 13329–13337. <https://doi.org/10.1029/JD094iD11p13329>
- da Silva, C. L., & Pasko, V. P. (2013). Dynamics of streamer-to-leader transition at reduced air densities and its implications for propagation of lightning leaders and gigantic jets. *Journal of Geophysical Research: Atmospheres*, 118(24), 13561–13590. <https://doi.org/10.1002/2013JD020618>
- da Silva, C. L., & Sao Sabbas, F. T. (2013). Consequences of the application of the streamer fluid model to the study of the sprite inception mechanism. *Advances in Space Research*, 51(10), 1902–1915. <https://doi.org/10.1016/j.asr.2012.11.025>
- Delanoë, J., & Hogan, R. J. (2010). Combined CloudSat-CALIPSO-MODIS retrievals of the properties of ice clouds. *Journal of Geophysical Research*, 115(D4), D00H29. <https://doi.org/10.1029/2009JD012346>
- Di Michele, S., McNally, T., Bauer, P., & Genkova, I. (2013). Quality assessment of cloud-top height estimates from satellite IR radiances using the CALIPSO Lidar. *IEEE Transactions on Geoscience and Remote Sensing*, 51(4), 2454–2464. <https://doi.org/10.1109/TGRS.2012.2210721>
- Dimitriadou, K., Chanrion, O., Neubert, T., Protat, A., Louf, V., Heumesser, M., et al. (2022). Analysis of blue corona discharges at the top of tropical thunderstorm clouds in different phases of convection. *Geophysical Research Letters*, 49(6), e2021GL095879. <https://doi.org/10.1029/2021GL095879>
- Ebert, U., & Sentman, D. D. (2008). Streamers, sprites, leaders, lightning: From micro- to macroscales. *Journal of Physics D: Applied Physics*, 41(23), 230301. <https://doi.org/10.1088/0022-3727/41/23/230301>
- Edens, H. E. (2011). Photographic and lightning mapping observations of a blue starter over a New Mexico thunderstorm. *Geophysical Research Letters*, 38(17), L17804. <https://doi.org/10.1029/2011GL048543>
- Goodman, S. J., Blakeslee, R. J., Koshak, W. J., Mach, D., Bailey, J., Buechler, D., et al. (2013). The GOES-R geostationary lightning mapper (GLM). *Atmospheric Research*, 125–126, 34–49. <https://doi.org/10.1016/j.atmosres.2013.01.006>
- Gordillo-Vázquez, F., & Pérez-Invernón, F. (2021). A review of the impact of transient luminous events on the atmospheric chemistry: Past, present, and future. *Atmospheric Research*, 252, 105432. <https://doi.org/10.1016/j.atmosres.2020.105432>
- Grandell, J., Stuhlmann, R., Dobber, M., Bennett, A., Biron, D., Defer, E., et al. (2010). EUMETSAT Meteorol Third Generation (MTG) lightning imager: From mission requirements to product development. In *AGU fall meeting abstracts* (Vol. 2010, p. AE21A-0257).
- Gryspeerd, E., Sourdeval, O., Quaas, J., Delanoë, J., Krämer, M., & Kühne, P. (2018). Ice crystal number concentration estimates from lidar-radar satellite remote sensing – Part 2: Controls on the ice crystal number concentration. *Atmospheric Chemistry and Physics*, 18(19), 14351–14370. <https://doi.org/10.5194/acp-18-14351-2018>
- Hagihara, Y., Okamoto, H., & Luo, Z. J. (2014). Joint analysis of cloud top heights from CloudSat and CALIPSO: New insights into cloud top microphysics. *Journal of Geophysical Research: Atmospheres*, 119(7), 4087–4106. <https://doi.org/10.1002/2013JD020919>
- Hersbach, H., Bell, B., Berrisford, P., Hirahara, S., Horányi, A., Muñoz-Sabater, J., et al. (2020). The ERA5 global reanalysis. *Quarterly Journal of the Royal Meteorological Society*, 146(730), 1999–2049. <https://doi.org/10.1002/qj.3803>
- Heumesser, M. (2021). The origin of gamma-ray flashes in thunderstorms (PhD thesis). Technical University of Denmark. Retrieved from <https://orbit.dtu.dk/en/publications/the-origin-of-gamma-ray-flashes-in-thunderstorms>
- Heumesser, M., Chanrion, O., Neubert, T., Christian, H. J., Dimitriadou, K., Gordillo-Vázquez, F. J., et al. (2021). Spectral observations of optical emissions associated with terrestrial gamma-ray flashes. *Geophysical Research Letters*, 48(4), 2020GL090700. <https://doi.org/10.1029/2020GL090700>
- Husbjerg, L. S., Neubert, T., Chanrion, O., Dimitriadou, K., Li, D., Stendel, M., et al. (2022). Observations of blue corona discharges in thunderclouds. *Geophysical Research Letters*, 49(12), e2022GL099064. <https://doi.org/10.1029/2022GL099064>
- International Civil Aviation Organization. (2002). World geodetic system - 1984 (WGS-84) manual, doc 9674-an/946 (Tech. Rep.) (2nd ed.).
- Karunarathne, S., Marshall, T. C., Stolzenburg, M., & Karunarathna, N. (2015). Observations of positive narrow bipolar pulses. *Journal of Geophysical Research: Atmospheres*, 120(14), 7128–7143. <https://doi.org/10.1002/2015JD023150>
- Kostinskiy, A. Y., Marshall, T. C., & Stolzenburg, M. (2020). The mechanism of the origin and development of lightning from initiating event to initial breakdown pulses (v.2). *Journal of Geophysical Research: Atmospheres*, 125(22), e2020JD033191. <https://doi.org/10.1029/2020JD033191>
- Li, D., Liu, F., Pérez-Invernón, F. J., Lu, G., Qin, Z., Zhu, B., & Luque, A. (2020). On the accuracy of ray-theory methods to determine the altitudes of intracloud electric discharges and ionospheric reflections: Application to narrow bipolar events. *Journal of Geophysical Research: Atmospheres*, 125(9), e2019JD032099. <https://doi.org/10.1029/2019JD032099>
- Li, D., Luque, A., Gordillo-Vázquez, F. J., Liu, F., Lu, G., Neubert, T., et al. (2021). Blue flashes as counterparts to narrow bipolar events: The optical signal of shallow in-cloud discharges. *Journal of Geophysical Research: Atmospheres*, 126(13), e2021JD035013. <https://doi.org/10.1029/2021JD035013>
- Li, D., Luque, A., Gordillo-Vázquez, F. J., Pérez-Invernón, F. J., Husbjerg, L. S., Neubert, T., et al. (2023). Different types of corona discharges associated with high-altitude positive narrow bipolar events nearby cloud top. *Journal of Geophysical Research: Atmospheres*, 128(4), e2022JD037883. <https://doi.org/10.1029/2022jd037883>
- Li, D., Luque, A., Gordillo-Vázquez, F. J., Silva, C. D., Krehbiel, P. R., Rachidi, F., & Rubinstein, M. (2022a). Secondary fast breakdown in narrow bipolar events. *Geophysical Research Letters*, 49(7), e2021GL097452. <https://doi.org/10.1029/2021GL097452>
- Li, D., Luque, A., Lehtinen, N. G., Gordillo-Vázquez, F. J., Neubert, T., Lu, G., et al. (2022b). Multi-pulse corona discharges in thunderclouds observed in optical and radio bands. *Geophysical Research Letters*, 49(13), e2022GL098938. <https://doi.org/10.1029/2022GL098938>
- Lidar Level 1 V4.10 Data Product Descriptions. (2016). Retrieved from https://www-calipso.larc.nasa.gov/resources/calipso_users_guide/data_summaries/11b/index_v4-x.php#tropopause_height. [Online].
- Light, T. E., Suszcynsky, D. M., Kirkland, M. W., & Jacobson, A. R. (2001). Simulations of lightning optical waveforms as seen through clouds by satellites. *Journal of Geophysical Research*, 106(D15), 17103–17114. <https://doi.org/10.1029/2001JD900051>
- Liu, C.-Y., Chiu, C.-H., Lin, P.-H., & Min, M. (2020). Comparison of cloud-top property retrievals from advanced Himawari imager, MODIS, CloudSat/CPR, CALIPSO/CALIP, and radiosonde. *Journal of Geophysical Research: Atmospheres*, 125(15), e2020JD032683. <https://doi.org/10.1029/2020JD032683>
- Liu, F., Lu, G., Neubert, T., Lei, J., Chanrion, O., Østgaard, N., et al. (2021a). Optical emissions associated with narrow bipolar events from thunderstorm clouds penetrating into the stratosphere. *Nature Communications*, 12(6631), 6631. <https://doi.org/10.1038/s41467-021-26914-4>

- Liu, F., Zhu, B., Lu, G., Lei, J., Shao, J., Chen, Y., et al. (2021b). Meteorological and electrical conditions of two mid-latitude thunderstorms producing blue discharges. *Journal of Geophysical Research: Atmospheres*, *126*(8), e2020JD033648. <https://doi.org/10.1029/2020JD033648>
- Liu, F., Zhu, B., Lu, G., Qin, Z., Lei, J., Peng, K.-M., et al. (2018). Observations of blue discharges associated with negative narrow bipolar events in active deep convection. *Geophysical Research Letters*, *45*(6), 2842–2851. <https://doi.org/10.1002/2017GL076207>
- Liu, N., Dwyer, J. R., Tilles, J. N., Stanley, M. A., Krehbiel, P. R., Rison, W., et al. (2019). Understanding the radio spectrum of thunderstorm narrow bipolar events. *Journal of Geophysical Research: Atmospheres*, *124*(17–18), 10134–10153. <https://doi.org/10.1029/2019JD030439>
- Liu, Z., Omar, A. H., Hu, Y., & Vaughan, M. A. (2005). CALIOP algorithm theoretical basis document Part 3: Scene classification algorithms.
- Liu, Z., Vaughan, M., Winker, D., Kittaka, C., Getzewich, B., Kuehn, R., et al. (2009). The CALIPSO lidar cloud and aerosol discrimination: Version 2 algorithm and initial assessment of performance. *Journal of Atmospheric and Oceanic Technology*, *26*(7), 1198–1213. <https://doi.org/10.1175/2009JTECHA1229.1>
- López, J. A., Montanyà, J., van der Velde, O., Romero, D., Gordillo-Vázquez, F. J., Pérez-Invernón, F. J., et al. (2022). Initiation of lightning flashes simultaneously observed from space and the ground: Narrow bipolar events. *Atmospheric Research*, *268*, 105981. <https://doi.org/10.1016/j.atmosres.2021.105981>
- Luque, A., & Ebert, U. (2009). Emergence of sprite streamers from screening-ionization waves in the lower ionosphere. *Nature Geoscience*, *2*(11), 757–760. <https://doi.org/10.1038/ngeo662>
- Luque, A., Gordillo-Vázquez, F. J., Li, D., Malagón-Romero, A., Pérez-Invernón, F. J., Schmalzried, A., et al. (2020). Modeling lightning observations from space-based platforms (CloudScat.jl 1.0). *Geoscientific Model Development*, *13*(11), 5549–5566. <https://doi.org/10.5194/gmd-13-5549-2020>
- Lyons, W. A., Nelson, T. E., Armstrong, R. A., Pasko, V. P., & Stanley, M. A. (2003). Upward electrical discharges from thunderstorm tops. *Bulletin of the American Meteorological Society*, *84*(4), 445–454. <https://doi.org/10.1175/BAMS-84-4-445>
- Lyu, F., Cummer, S. A., Qin, Z., & Chen, M. (2019). Lightning initiation processes imaged with very high frequency broadband interferometry. *Journal of Geophysical Research: Atmospheres*, *124*(6), 2994–3004. <https://doi.org/10.1029/2018JD029817>
- MacGorman, D. R., Elliott, M. S., & DiGangi, E. (2017). Electrical discharges in the overshooting tops of thunderstorms. *Journal of Geophysical Research: Atmospheres*, *122*(5), 2929–2957. <https://doi.org/10.1002/2016JD025933>
- Marshall, T., Bandara, S., Karunarathne, N., Karunarathne, S., Kolmasova, I., Siedlecki, R., & Stolzenburg, M. (2019). A study of lightning flash initiation prior to the first initial breakdown pulse. *Atmospheric Research*, *217*, 10–23. <https://doi.org/10.1016/j.atmosres.2018.10.013>
- Mitchell, D. L., Garnier, A., Pelon, J., & Erfani, E. (2018). CALIPSO (IIR–CALIOP) retrievals of cirrus cloud ice-particle concentrations. *Atmospheric Chemistry and Physics*, *18*(23), 17325–17354. <https://doi.org/10.5194/acp-18-17325-2018>
- Montanyà, J., López, J. A., Morales Rodríguez, C. A., van der Velde, O. A., Fabró, F., Pineda, N., et al. (2021). A simultaneous observation of lightning by ASIM, Colombia-lightning mapping array, GLM, and ISS-LIS. *Journal of Geophysical Research: Atmospheres*, *126*(6), e2020JD033735. <https://doi.org/10.1029/2020JD033735>
- Neubert, T., Chanrion, O., Heumesser, M., Dimitriadou, K., Husbjerg, L., Rasmussen, I. L., et al. (2021). Observation of the onset of a blue jet into the stratosphere. *Nature*, *589*(7842), 371–375. <https://doi.org/10.1038/s41586-020-03122-6>
- Neubert, T., Østgaard, N., Reglero, V., Blanc, E., Chanrion, O., Oxborrow, C. A., et al. (2019). The ASIM mission on the international space station. *Space Science Reviews*, *215*(2), 1–17. <https://doi.org/10.1007/s11214-019-0592-z>
- Nijdam, S., Teunissen, J., & Ebert, U. (2020). The physics of streamer discharge phenomena. *Plasma Sources Science and Technology*, *29*(10), 103001. <https://doi.org/10.1088/1361-6595/abaa05>
- O'Neill, M. E., Orf, L., Heymsfield, G. M., & Halbert, K. (2021). Hydraulic jump dynamics above supercell thunderstorms. *Science*, *373*(6560), 1248–1251. <https://doi.org/10.1126/science.abh3857>
- Pasko, V. P. (2008). Blue jets and gigantic jets: Transient luminous events between thunderstorm tops and the lower ionosphere. *Plasma Physics and Controlled Fusion*, *50*(12), 124050. <https://doi.org/10.1088/0741-3335/50/12/124050>
- Pucik, T., Groenemeijer, P., & Tsonevsky, I. (2021). *Vertical wind shear and convective storms* (Tech. Rep. No. 879). ECMWF. <https://doi.org/10.21957/z0b3t5mrv>
- Raizer, Y. P., & Allen, J. E. (1991). *Gas discharge physics* (Vol. 1). Springer.
- Rison, W., Krehbiel, P. R., Stock, M. G., Edens, H. E., Shao, X.-M., Thomas, R. J., et al. (2016). Observations of narrow bipolar events reveal how lightning is initiated in thunderstorms. *Nature Communications*, *7*(1), 10721. [https://doi.org/10.1038/ncomms10721\(2016\)](https://doi.org/10.1038/ncomms10721(2016))
- Smith, D. A., Heavner, M. J., Jacobson, A. R., Shao, X. M., Massey, R. S., Sheldon, R. J., & Wiens, K. C. (2004). A method for determining intracloud lightning and ionospheric heights from VLF/LF electric field records. *Radio Science*, *39*(1), RS1010. <https://doi.org/10.1029/2002RS002790>
- Smith, D. A., Shao, X. M., Holden, D. N., Rhodes, C. T., Brook, M., Krehbiel, P. R., et al. (1999). A distinct class of isolated intracloud lightning discharges and their associated radio emissions. *Journal of Geophysical Research*, *104*(D4), 4189–4212. <https://doi.org/10.1029/1998JD200045>
- Soler, S., Gordillo-Vázquez, F. J., Pérez-Invernón, F. J., Luque, A., Li, D., Neubert, T., et al. (2021). Global frequency and geographical distribution of nighttime streamer corona discharges (BLUEs) in thunderclouds. *Geophysical Research Letters*, *48*(18), e2021GL094657. <https://doi.org/10.1029/2021GL094657>
- Soler, S., Pérez-Invernón, F. J., Gordillo-Vázquez, F. J., Luque, A., Li, D., Malagón-Romero, A., et al. (2020). Blue optical observations of narrow bipolar events by ASIM suggest corona streamer activity in thunderstorms. *Journal of Geophysical Research: Atmospheres*, *125*(16), e2020JD032708. <https://doi.org/10.1029/2020JD032708>
- Sourdeval, O., Gryspeerdt, E., Krämer, M., Goren, T., Delanoë, J., Afchine, A., et al. (2018). Ice crystal number concentration estimates from lidar–radar satellite remote sensing – Part 1: Method and evaluation. *Atmospheric Chemistry and Physics*, *18*(19), 14327–14350. <https://doi.org/10.5194/acp-18-14327-2018>
- Stolzenburg, M., & Marshall, T. C. (2009). Electric field and charge structure in lightning-producing clouds. In H. D. Betz, U. Schumann, & P. Laroche (Eds.), *Lightning: Principles, instruments and applications: Review of modern lightning research* (pp. 57–82). Springer Netherlands. https://doi.org/10.1007/978-1-4020-9079-0_3
- Stolzenburg, M., Rust, W. D., & Marshall, T. C. (1998). Electrical structure in thunderstorm convective regions: 3. Synthesis. *Journal of Geophysical Research*, *103*(D12), 14097–14108. <https://doi.org/10.1029/97JD03545>
- Thomson, L. W., & Krider, E. P. (1982). The effects of clouds on the light produced by lightning. *Journal of the Atmospheric Sciences*, *39*(9), 2051–2065. [https://doi.org/10.1175/1520-0469\(1982\)039<2051:TEOCOT>2.CO;2](https://doi.org/10.1175/1520-0469(1982)039<2051:TEOCOT>2.CO;2)
- Tilles, J. N., Liu, N., Stanley, M. A., Krehbiel, P. R., Rison, W., Stock, M. G., et al. (2019). Fast negative breakdown in thunderstorms. *Nature Communications*, *10*(1), 1–12. <https://doi.org/10.1038/s41467-019-09621-z>
- Walker, T. D., & Christian, H. J. (2019). Triggered lightning spectroscopy: 2. A quantitative analysis. *Journal of Geophysical Research: Atmospheres*, *124*(7), 3930–3942. <https://doi.org/10.1029/2018JD029901>
- Wang, P. K., Cheng, K.-Y., Setvak, M., & Wang, C.-K. (2016). The origin of the gullwing-shaped cirrus above an Argentinian thunderstorm as seen in CALIPSO images. *Journal of Geophysical Research: Atmospheres*, *121*(7), 3729–3738. <https://doi.org/10.1002/2015JD024111>

- Wescott, E. M., Sentman, D. D., Heavner, M. J., Hampton, D. L., Osborne, D. L., & Vaughan, O. H., Jr. (1996). Blue starters brief upward discharges from an intense Arkansas thunderstorm. *Geophysical Research Letters*, *23*(16), 2153–2156. <https://doi.org/10.1029/96GL01969>
- Wescott, E. M., Sentman, D. D., Stenbaek-Nielsen, H. C., Huet, P., Heavner, M. J., & Moudry, D. R. (2001). New evidence for the brightness and ionization of blue starters and blue jets. *Journal of Geophysical Research*, *106*(A10), 21549–21554. <https://doi.org/10.1029/2000JA000429>
- Winker, D., Pelon, J., Coakley, J., Jr., Ackerman, S., Charlson, R., Colarco, P., et al. (2010). The CALIPSO mission: A global 3D view of aerosols and clouds. *Bulletin of the American Meteorological Society*, *91*(9), 1211–1230. <https://doi.org/10.1175/2010BAMS3009.1>
- Wu, T., Dong, W., Zhang, Y., Funaki, T., Yoshida, S., Morimoto, T., et al. (2012). Discharge height of lightning narrow bipolar events. *Journal of Geophysical Research*, *117*(D5), D05119. <https://doi.org/10.1029/2011JD017054>
- Wu, T., Yoshida, S., Ushio, T., Kawasaki, Z., & Wang, D. (2014). Lightning-initiator type of narrow bipolar events and their subsequent pulse trains. *Journal of Geophysical Research: Atmospheres*, *119*(12), 7425–7438. <https://doi.org/10.1002/2014JD021842>
- Yang, J., Zhang, Z., Wei, C., Lu, F., & Guo, Q. (2017). Introducing the new generation of Chinese geostationary weather satellites, Fengyun-4. *Bulletin of the American Meteorological Society*, *98*(8), 1637–1658. <https://doi.org/10.1175/BAMS-D-16-0065.1>
- Zhao, L., Wang, S.-Y. S., Becker, E., Yoon, J.-H., & Mukherjee, A. (2020). Cyclone Fani: The tug-of-war between regional warming and anthropogenic aerosol effects. *Environmental Research Letters*, *15*(9), 094020. <https://doi.org/10.1088/1748-9326/ab91e7>
- Zhu, Y., Bitzer, P., Rakov, V., & Ding, Z. (2021). A machine-learning approach to classify cloud-to-ground and intracloud lightning. *Geophysical Research Letters*, *48*(1), e2020GL091148. <https://doi.org/10.1029/2020GL091148>
- Zhu, Y., Rakov, V. A., Tran, M. D., Stock, M. G., Heckman, S., Liu, C., et al. (2017). Evaluation of ENTLN performance characteristics based on the ground truth natural and rocket-triggered lightning data acquired in Florida. *Journal of Geophysical Research: Atmospheres*, *122*(18), 9858–9866. <https://doi.org/10.1002/2017JD027270>
- Zhu, Y., Stock, M., Lapierre, J., & DiGangi, E. (2022). Upgrades of the Earth networks total lightning network in 2021. *Remote Sensing*, *14*(9), 2209. <https://doi.org/10.3390/rs14092209>